© 2018. Published by The Company of Biologists Ltd | Journal of Cell Science (2018) 131, jcs214411. doi:10.1242/jcs.214411

RESEARCH ARTICLE

H2AFX and MDC1 promote maintenance of genomic integrity in male germ cells

Erika Testa[1], Daniela Nardozi[1], Cristina Antinozzi[1,*,‡], Monica Faieta[1,‡], Stefano Di Cecca[1], Cinzia Caggiano[1], Tomoyuki Fukuda[2,3], Elena Bonanno[4], Lou Zhenkun[5], Andros Maldonado[6,7], Ignasi Roig[6,7], Monica Di Giacomo[8] and Marco Barchi[1,§]

ABSTRACT

In somatic cells, *H2afx* and *Mdc1* are close functional partners in DNA repair and damage response. However, it is not known whether they are also involved in the maintenance of genome integrity in meiosis. By analyzing chromosome dynamics in *H2afx*$^{-/-}$ spermatocytes, we found that the synapsis of autosomes and X-Y chromosomes was impaired in a fraction of cells. Such defects correlated with an abnormal recombination profile. Conversely, *Mdc1* was dispensable for the synapsis of the autosomes and played only a minor role in X-Y synapsis, compared with the action of *H2afx*. This suggested that those genes have non-overlapping functions in chromosome synapsis. However, we observed that both genes play a similar role in the assembly of MLH3 onto chromosomes, a key step in crossover formation. Moreover, we show that *H2afx* and *Mdc1* cooperate in promoting the activation of the recombination-dependent checkpoint, a mechanism that restrains the differentiation of cells with unrepaired DSBs. This occurs by a mechanism that involves P53. Overall, our data show that, in male germ cells, *H2afx* and *Mdc1* promote the maintenance of genome integrity.

This article has an associated First Person interview with the first author of the paper.

KEY WORDS: *H2afx*, *Mdc1*, Crossover, X-Y, Meiosis, Checkpoint

INTRODUCTION

The production of gametes with an intact haploid genome is crucial for the prevention of birth defects. It depends on the formation of crossovers (COs), the chromosome connections that ensure faithful segregation during metaphase I (Keeney, 2008). CO formation is achieved by meiotic recombination, a process that is initiated with the introduction of double-strand breaks (DSBs) by the SPO11 protein. DSBs are potentially dangerous because they introduce opportunities for generating gross chromosomal rearrangements that may be detrimental to germ cell genome integrity (Kim et al., 2016). In addition, as in many organisms, SPO11-induced DNA damage in mammals is coupled with synapsis of homologous chromosomes (homologs) (Bolcun-Filas and Schimenti, 2012). Failure to recombine can cause aneuploidy and lead to the development of an embryo with an unbalanced chromosome number. In order to avoid such dangerous outcomes, surveillance mechanisms (or checkpoints) sense defects in meiotic recombination/synapsis, and arrest the progression of cells with unresolved problems.

In male mice, the meiotic progression of germ cells is monitored by two main distinct mechanisms: the sex body-deficient checkpoint and the recombination (or DNA damage)-dependent checkpoint. The former is triggered in synapsis-defective cells by faulty transcriptional silencing of X-Y-associated genes that are toxic to male germ cells (Mahadevaiah et al., 2008; Burgoyne et al., 2009; Royo et al., 2010). The latter is instead activated in cells that have an abnormal recombination profile. In early pachynema cells, it co-ordinates DSBs repair with meiotic progression, preventing differentiation to mid-pachynema, until a sufficient number of DSBs have been repaired (e.g. as in *Tex19.1*$^{-/-}$ spermatocytes; Crichton et al., 2017 preprint) or, ultimately, causing apoptosis if DSBs cannot be properly resolved (e.g. if they lack TRIP13, an AAA+ ATPase required to timely complete meiotic recombination; Pacheco et al., 2015). Genetic evidence indicates that activation of the recombination-dependent checkpoint depends on the activity of the DNA damage sensor kinase ATM (ataxia-telangiectasia mutated), its downstream target CHK2 (Pacheco et al., 2015), and P53/TAp63 family members (Marcet-Ortega et al., 2017).

In somatic cells, checkpoint response to DNA damage entails a functional interplay between H2AFX (nucleosomal variant histone H2AX), MDC1 (mediator of DNA damage checkpoint protein 1) and ATM. ATM-mediated phosphorylation of H2AFX (which is referred to as γH2AFX) is one of the earliest responses to damage (Rogakou et al., 1998; Rogakou et al., 1999). MDC1 binding onto γH2AFX promotes ATM accumulation at the sites of DNA damage. This amplifies the DNA damage signals (Lou et al., 2006), including activation of the ATM target P53 (Canman et al., 1998; Khanna et al., 1998; Banin et al., 1998). Another key response to DNA damage is DNA repair. In this respect, γH2AFX and MDC1 have been found to promote DNA repair by homologous recombination (Ünal et al., 2004; Xie et al., 2004, 2007; Sonoda et al., 2007; Zhang et al., 2005), a process that ensures repair of DNA damage and synapsis of the homologs in mammalian meiosis.

[1]Department of Biomedicine and Prevention, Section of Anatomy, University of Rome Tor Vergata, 00133 Rome, Italy. [2]Department of Cellular Physiology, Niigata University Graduate School of Medical and Dental Sciences, 951-8510 Niigata, Japan. [3]Graduate School of Biological Sciences, Nara Institute of Science and Technology, 630-0192 Nara, Japan. [4]Department of Experimental Medicine and Surgery, Section of Pathological Anatomy, University of Rome Tor Vergata, 00133 Rome, Italy. [5]Division of Oncology Research, Department of Oncology, Mayo Clinic, Rochester, MN 55905 USA. [6]Genome Integrity and Instability Group, Institut de Biotecnologia i Biomedicina, Universitat Autònoma de Barcelona, 08193 Cerdanyola del Vallès, Spain. [7]Department of Cell Biology, Physiology and Immunology, Universitat Autònoma de Barcelona, 08193 Cerdanyola del Vallès, Spain. [8]European Molecular Biology Laboratory (EMBL), 00015 Rome, Italy.
*Present address: Department of Movement, Human and Health Sciences, University of Rome Foro Italico, 00015 Rome, Italy.
‡These authors contributed equally to this work

[§]Author for correspondence (marco.barchi@uniroma2.it)

E.T., 0000-0002-0101-2973; D.N., 0000-0001-9660-7509; C.A., 0000-0003-4296-5081; M.F., 0000-0002-1304-4542; C.C., 0000-0002-2381-1848; T.F., 0000-0003-2069-7127; E.B., 0000-0002-0222-0141; A.M., 0000-0001-8322-8390; I.R., 0000-0003-0313-3581; M. D.G., 0000-0002-4075-0725; M.B., 0000-0003-1104-6234

Received 15 December 2017; Accepted 31 January 2018

Journal of Cell Science (2018) 131, jcs214411. doi:10.1242/jcs.214411

However, whether H2AFX and MDC1 play a function in checkpoint response and meiotic recombination in meiotic cells is unclear.

By comparing the phenotype of *H2afx* and *Mdc1* mutants, we demonstrated that DSBs form at normal levels in both mutants. However, in the absence of *H2afx*, the assembly of MSH4 foci and synapsis of the autosomes are impaired. On the contrary, such defects are not observed in $Mdc1^{-/-}$ spermatocytes, which indicates that *H2afx* and *Mdc1* are functionally separated in recombination-mediated synapsis. Accordingly, X-Y asynapsis was much higher in $H2afx^{-/-}$ spermatocytes than in *Mdc1* mutant cells. Therefore, *Mdc1* also performs a minor function in recombination-mediated synapsis of the sex chromosomes. Beside such differences, H2AFX and MDC1 play a similar role in promoting the assembly of MLH3 foci (a marker of CO formation). This points to a role of these genes in the pathway that enables stable interaction and segregation of the homologs at metaphase I. Furthermore, we showed evidence that both H2AFX and MDC1 also play a role in the activation of the recombination-dependent checkpoint, promoting the activation of P53.

Overall, these data highlight that *H2afx* and *Mdc1* sustain genome integrity preservation of male germ cells, by both promoting proper processing of DSBs and delaying the progression of cells with unrepaired damage.

RESULTS

H2afx and *Mdc1* are dispensable for regulation of nucleus-wide DSBs

In mammalian meiocytes, the activity of the PI3K-like kinase ATM is essential to constrain the formation of nucleus-wide DSBs by SPO11 (Lange et al., 2011). Therefore, targets of ATM are expected to exert control of DSB formation. In mouse meiosis, H2AFX is phosphorylated by ATM at leptonema and zygonema, as a response to DSBs formation (Barchi et al., 2005; Bellani et al., 2005). In addition, the γH2AFX binding partner MDC1 is also a target of ATM (Matsuoka et al., 2007; Lavin and Kozlov, 2007; Jungmichel et al., 2012). However, whether H2AFX or MDC1 take part of the regulatory mechanism that controls the function of SPO11 in meiosis is unknown. To assess nucleus-wide DSBs formation in $H2afx^{-/-}$ males, we quantified SPO11–oligonucleotide complexes that are a byproduct of meiotic DSB formation (Pan et al., 2011; Neale et al., 2005; Lange et al., 2011). As $H2afx^{-/-}$ spermatocytes undergo apoptosis at mid-pachynema (Fernandez-Capetillo et al., 2003; Mahadevaiah et al., 2008), this experiment was performed using testicles of 12.5 days post-partum (dpp) mice, in which cells are expected to have progressed up to early pachynema. Quantification of the steady-state level of SPO11–oligonucleotide complexes in a single experiment revealed a small weakening of the signal in $H2afx^{-/-}$ testes compared with that in the control (71.2% of wild type) (Fig. 1A). This may reflect stochastic variability in the samples or, alternatively, be due to a reduction of DSBs in the mutant. In order to make a distinction between those two options, we quantified DSBs by counting DMC1 foci in leptonema and early to mid-zygonema cells. DMC1 is a meiosis-specific member of the bacterial RecA protein family, which stabilizes strand exchange intermediates to promote DSB repair (Bishop et al., 1992; Yoshida et al., 1998). Cytologically, it can be seen as foci along meiotic chromosome axes, and has been broadly used as a surrogate marker for DSB formation (Lam and Keeney, 2015). We detected no differences between $H2afx^{-/-}$ and wild-type genotypes (Fig. 1B, Table S1), which suggests that in absence of *H2afx*, SPO11 activity is not altered. This was confirmed by quantifying the number of BRCA1 foci, a DNA-repair protein that we found assembled onto meiotic chromosomes following DSB formation (Fig. S1A,B, Table S1). Importantly, similar to $H2afx^{-/-}$ spermatocytes, we observed that in *Mdc1*-knockout spermatocytes, the number of DMC1 foci was not different compared with controls (Fig. 1B). Hence, we concluded that H2AFX and MDC1 are dispensable for the ATM-mediated homeostatic control of DSBs.

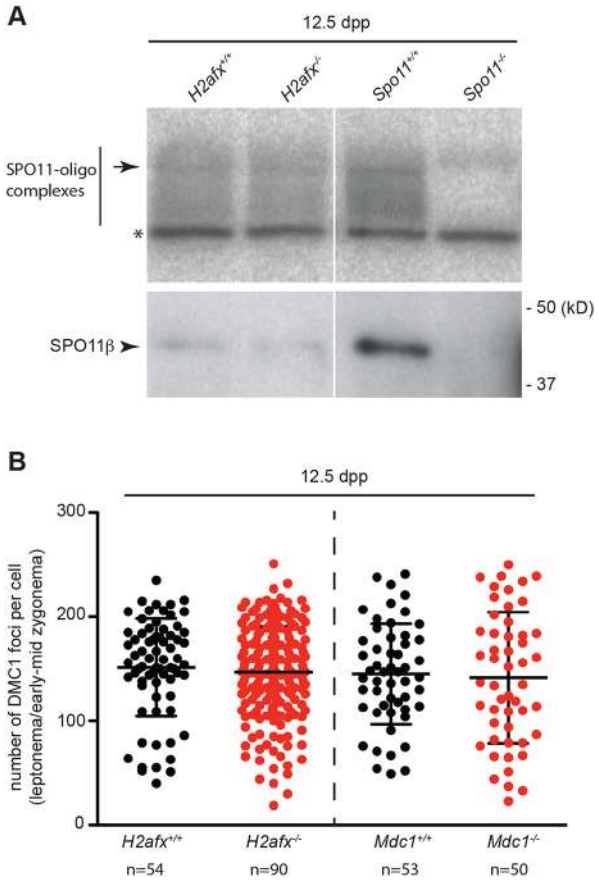

Fig. 1. *H2Afx* and *Mdc1* are dispensable for the formation and homeostatic control of DSBs. (A) Autoradiography of SPO11–oligonucleotide complexes (top) and anti-SPO11 western detection (bottom) isolated by immunoprecipitation of juvenile mice testis. Asterisk indicates non-specific terminal transferase labeling; arrow represents migration position of immunoglobulin heavy chain. (B) Quantification of DMC1 foci number in spermatocytes of the indicated genotypes. Each dot in the graph indicates the number of DMC1 foci per nucleus; *n*=3 mice analyzed per genotype; the error bars are means and s.d., *n*=number of cells analyzed.

Defective X-Y chromosome synapsis in $H2afx^{-/-}$ and $Mdc1^{-/-}$ cells do not rely on reduced formation of DSBs in the PAR

During meiotic prophase I, synapsis of the homologs occurs gradually and it is completed by pachynema. At this stage, the autosomes are fully synapsed along their lengths; conversely, X-Y chromosome synapsis is restricted to the pseudo autosomal region (PAR), a small region of homology between them (Perry et al., 2001). As the PAR is small, the X-Y chromosome pair is very sensitive to perturbations of the synaptic process. Confirming a previous report (Fernandez-Capetillo et al., 2003), we found that lack of *H2afx* causes an X-Y chromosome synapsis defect in about 80% of the pachynema cells in juvenile males (Fig. S1C,D). This indicates that DSB formation and/or recombination within the PAR is perturbed. However, the mechanisms underlying this defect are not known.

Journal of Cell Science (2018) 131, jcs214411. doi:10.1242/jcs.214411

In mice, DSB formation within the PAR requires proper expression of *Spo11* splicing variants (Kauppi et al., 2011). To investigate their expression in the *H2afx* mutant, we amplified the cDNA of 10.5 dpp *H2afx*$^{-/-}$ and wild-type testis, using *Spo11* isoform-specific primers. We observed that *Spo11β*, *Spo11α*, *Bcl*I and *Sph*I isoforms (Keeney et al., 1999) were expressed in the mutant at a level comparable with that of the control (Fig. 2A). Thus, X-Y chromosome asynapsis in the mutant is unrelated to changes in *Spo11* splicing pattern.

Formation of DSBs within the PAR relies also on the structural characteristics of the PAR. PAR axes in mice are disproportionally long relative to DNA length. This results in shorter chromatin loops, with a consequent increase in the potential for DSBs (Kauppi et al., 2011). H2AFX is a structural component of chromatin. We therefore conjectured that its absence might cause an increase in the size of PAR-associated chromatin loops. To evaluate this possibility, we compared the PAR chromatin loop size of wild-type and *H2afx*$^{-/-}$ spermatocytes in chromosome spreads of early pachynema nuclei. Early substages of pachynema were identified by co-staining the chromosomes with the anti-DMC1 antibody, a marker that, in normal cells, persists in relatively high quantities up to early pachynema. As a proxy for loop size, we measured fluorescence *in situ* hybridization (FISH) signal extension from axes of cells, using a PAR-specific probe (Fig. 2B). Under our experimental conditions, we could always unambiguously distinguish the Y-PAR, whereas the X-PAR signals were often weak and sometimes not visible (Fig. S1E). Therefore, we focused our analyses on the Y-PAR. We observed that the loop size of unsynapsed Y chromosomes of *H2afx*$^{-/-}$ cells at early pachynema was not enlarged compared with that measured in synapsed Y chromosomes of wild-type or *H2afx*$^{-/-}$ cells (Fig. 2C). Actually, we rather measured a slight size reduction, indicating that the asynapsis of the X-Y chromosomes is not linked to changes in chromatin loop organization. Based on these observations, we hypothesized that in *H2afx*$^{-/-}$ spermatocytes, DSBs occur within the Y-PAR, at the wild-type level. Thus, using DMC1 as a marker, we analyzed DSB formation within the PAR. Our analyses revealed that in the mutant, a DMC1 focus was observed within the Y-PAR of asynapsed chromosomes at early pachynema in 66.6±9% (n=30) of the nuclei

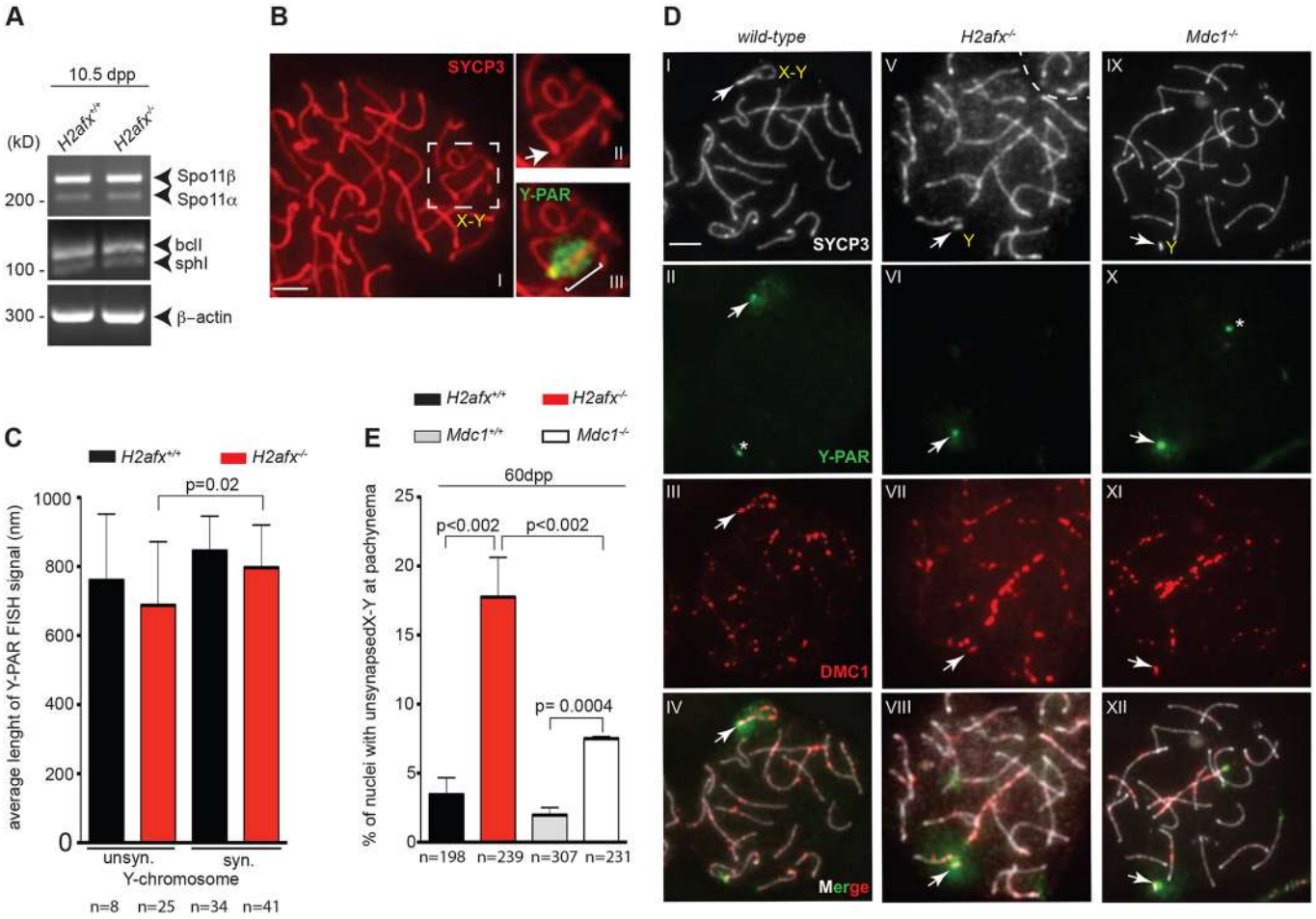

Fig. 2. X-Y chromosome asynapsis in *H2afx*$^{-/-}$ and *Mdc1*$^{-/-}$ cells does not rely on reduced formation of DSBs in the PAR. (A) RT-PCR analysis of *Spo11* splicing variants in the indicated genotypes. Level of β-actin was used as loading control. (B) Representative image of synapsed X-Y chromosomes in wild-type spermatocytes at early pachytene stage (I). SYCP3 marks the axial element of the SC. Magnification in II shows the X-Y chromosomes (dotted square in I). The arrow indicates the PAR region. Magnification in III shows the FISH signal identifying the Y-PAR region. The white bar indicates the extension of the PAR-FISH signal that is measured as a proxy for chromatin loop length. (C) Quantification of the average length of Y-PAR FISH signal among spermatocytes of indicated genotypes, with unsynapsed (unsyn.) and synapsed (syn.) Y chromosome (n=3 mice analyzed per genotype). (D) Representative early pachytene spermatocytes of indicated genotypes, labeled with anti-SYCP3 (I,V,IX), Y-PAR probe (II,VI,X) and anti-DMC1 antibody (III,VII,XI). White arrows indicate Y-PAR, while asterisks indicate a non-specific signal of the FISH. Merge images (IV,VIII,XII) show the localization of DMC1 foci within the Y-PAR region. (E) Quantification of nuclei with unsynapsed X-Y chromosomes at the pachynema stage in adult mice of the indicated genotypes (n=3 mice analyzed per genotype). Data are mean±s.d.; n=number of cells analyzed. Scale bars: 5 µm.

Journal of Cell Science (2018) 131, jcs214411. doi:10.1242/jcs.214411

(Fig. 2DI–VIII). This percentage closely matches that of the nuclei with Y-PAR associated foci at late zygonema in wild-type (Kauppi et al., 2011), indicating that a lack of H2AFX does not affect DSB formation within the PAR.

Previous findings showed that, in addition to *H2afx*, X-Y synapsis also requires *Mdc1* (Ichijima et al., 2011). Therefore, we quantified the number of PAR-associated DMC1 foci in *Mdc1*$^{-/-}$ cells. Similarly to what was observed in *H2afx*$^{-/-}$ spermatocytes, DSBs were present within the Y-PAR in 66±10% (*n*=28) of cases (Fig. 2DIX–XII), thus ruling out a defect in DSB formation. Interestingly, the side-by-side analyses of X-Y chromosome asynapsis frequency in adult mice from both *H2afx* and *Mdc1* mutants revealed that, although in *Mdc1*$^{-/-}$ spermatocytes the percentage of asynapsed chromosomes increased significantly relative to the wild-type, such an increase was much smaller compared with that observed in *H2afx*$^{-/-}$ cells (Fig. 2E). This indicates that, although both genes play a role in promoting the synapsis of sex chromosomes, the *H2afx* function predominates over that of *Mdc1*. Overall, these observations demonstrate that *H2afx* and *Mdc1* are not necessary for the formation of DSBs within PAR. However, both genes play a role in promoting X-Y synapsis, probably through mechanisms that are only partially overlapping (see Discussion).

H2afx$^{-/-}$ spermatocytes display defects in initiating both autosomes and X-Y chromosomes synapsis

The above observation that in the *H2afx*$^{-/-}$ mutant, X-Y synapsis is impaired in most cells, while DSBs form in normal number, suggests that this genotype might suffer from a defect in recombination-mediated synapsis. To test this hypothesis, we asked whether global autosome synapsis was also perturbed. In mice, the synapsis of the autosomes is initiated at zygonema. Cytologically, progression from leptonema to early zygonema is characterized by the assembly of SYCP1, which occurs when the elongation of the axial (now referred to as lateral) element containing SYCP3 has already begun (Fig. 3AI). As cells progress to mid-zygonema, the elongation of the chromosome axes is completed, and chromosome synapsis further extended coordinately in most of the chromosomes, up to 50% of chromosome length (Fig. 3AII). At late-zygonema, homologous synapsis extends over 50% of the chromosome length (Fig. 3AIII), and it is completed at pachynema (Fig. 3AIV).

A detailed analysis of autosome synapsis in *H2afx*$^{-/-}$ spermatocytes from adult mice revealed that a relevant fraction of cells at zygonema displayed defects in chromosome synapsis of the autosomes (henceforth referred to as zygonema-like cells) (Fig. 3B), with different characteristics. Specifically, 23% of zygotene-stage

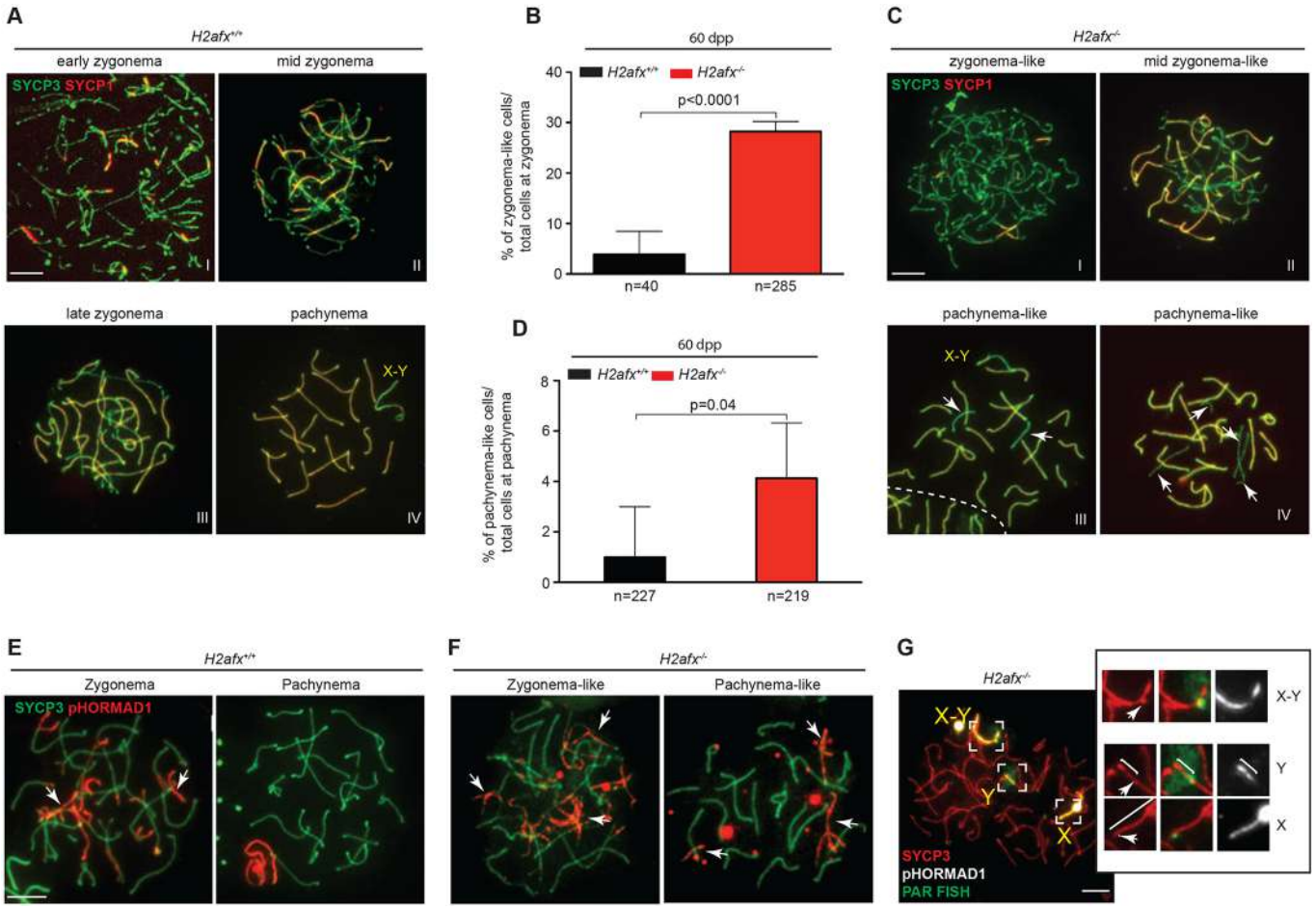

Fig. 3. Homologous synapsis of the autosomes is defective in *H2afx*$^{-/-}$ spermatocytes. (A,C) Representative images of nuclear spreads of the indicated stages, from wild-type and *H2afx*$^{-/-}$ spermatocytes labeled with anti-SYCP3 and anti-SYCP1 antibodies. Arrows indicate axes of unsynapsed chromosomes. (B,D) Quantification *of* zygonema-like cells (B) and pachynema-like cells (D) in mice of indicated genotypes (*H2afx*$^{+/+}$, *n*=3 mice; *H2afx*$^{-/-}$, *n*=4 mice). Data are mean±s.d.; *n*=number of cells analyzed. (E,F) Representative images of nuclear spreads of spermatocytes from the indicated stages and genotypes, labeled with anti-SYCP3 and anti-pHORMAD1 antibodies. Arrows indicate axes of unsynapsed homologs. (G) Representative image of *H2afx*$^{-/-}$ spread spermatocytes labeled with anti-SYCP3, anti-pHORMAD1 and FISH to identify the Y-PAR probe. Magnifications of dotted squares representing the pattern of pHORMAD1 in synapsed (top) and unsynapsed sex chromosomes (bottom) are shown on the right. White bars indicate the extension of Y and X chromosomes. Scale bars: 5 µm.

Journal of Cell Science (2018) 131, jcs214411. doi:10.1242/jcs.214411

cells displayed signs of delayed initiation of synapsis, or synapsis asynchrony in different homolog pairs. The former appeared as nuclei with fully elongated SYCP3-positive axes, with very limited synapsis (Fig. 3CI). The latter cells were instead characterized by multiple fully-asynapsed bivalents in the presence of at least two fully-synapsed homolog pairs (Fig. 3CII). In addition to such global defects in the initiation or coordinate extension of chromosome synapsis, in a restricted population of spermatocytes at zygonema (5.3%), we found cells with interstitial asynapsis (a 'bubble') (Fig. S2AI) and cells displaying non-homologous synapsis (Fig. S2AII,III). Non-homologous synapsis and bubbles were also observed concomitantly with the development of asynchronous synapsis in 5.4% of the cases.

There were also synaptic abnormalities at pachynema (Fig. 3D, Fig. S2B). Pachynema-like spermatocytes appeared as cells with only one or two pairs of unsynapsed autosomes in the presence of either synapsed (Fig. 3CIII) or asynapsed sex chromosomes (Fig. 3CIV). Notably, as previously described by others (Ichijima et al., 2011), we observed that in *Mdc1*$^{-/-}$ spermatocytes, autosome synapsis was substantially normal (zygotene/pachytene-like cells, wt: 0%, n=279; *Mdc1*$^{-/-}$: 1±1%, n=289), thus excluding any significant role of this gene in this process.

The presence of asynapsed chromosomes at zygonema and pachynema in the *H2afx*$^{-/-}$ mutant indicated that H2AFX might be required to either initiate synapsis of the autosomes, or to prevent their precocious dissociation. To distinguish between these two options, we took advantage of the phosphorylation status of the HORMA (Hop1, Rev7 and Mad2) domain 1 (HORMAD1) protein on chromosome axes through prophase I. In mice, HORMAD1 protein phosphorylation at Ser^{375} (an ATM/ATR kinases consensus site) occurs on unsynapsed, but not de-synapsed chromosomal regions (Fukuda et al., 2012). This makes HORMAD1 pSer^{375} (pHORMAD1) a reliable marker to distinguish between chromosomes showing asynapsis or de-synapsis defects. We first verified that lack of *H2afx* did not impact HORMAD protein deposition (Fig. S3A,B), global phosphorylation of HORMAD1 or that of other chromosome axes components, potential targets of ATM (Fukuda et al., 2012) (Fig. S3C,D). Then, we examined the chromosomal localization of pHORMAD1 using meiotic chromosome spread preparations. In the wild type, pHORMAD1 staining followed the pattern described previously (Fig. 3E) (Fukuda et al., 2012). In the *H2afx* mutant, asynapsed chromosomes of zygonema-like and pachynema-like cells were always phosphorylated (Fig. 3F). Moreover, the pHORMAD1 signal was also always present within the PAR of asynapsed X-Y chromosomes at pachynema (Fig. 3G). From these observations we inferred that both autosomes and sex chromosomes failed to initiate synapsis. Hence, we concluded that *H2afx* is required for the proper establishment of physical interaction between the homologs.

A fraction of *H2afx*$^{-/-}$ spermatocytes are eliminated by apoptosis before the completion of autosomal synapsis

In mice, spermatogenesis occurs within the seminiferous tubules in which, based on the specific germ cell association within each cross section, 12 epithelial stages (I–XII) can be identified (Russell et al., 1990; Ahmed and de Rooij, 2009). In the context of seminiferous epithelium, the lifespan of a spermatocyte that is unable to complete recombination and synapsis of the autosomes (e.g. if it lacks the strand-exchange protein DMC1) is extended until the cells reach epithelial stage IV, a stage equivalent to mid-pachynema in the wild type (Barchi et al., 2005; Mahadevaiah et al., 2008; Burgoyne et al., 2009). Confirming previous observations (Mahadevaiah et al., 2008), our histological analyses of *H2afx*$^{-/-}$ mice testis revealed that most spermatocytes were eliminated by apoptosis at epithelial stage IV (Fig. S4A). However, whether cells undergoing apoptosis reach stage IV and die before completion of autosome synapsis is currently unknown. To test this, we performed terminal deoxynucleotidyl transferase dUTP nick end labeling (TUNEL) on cells stained for SYCP3 or SYCP1. The analyses revealed that in *H2afx*$^{-/-}$ mice, in addition to cells where autosomes were fully paired along their length (i.e. pachytene stage spermatocytes), the TUNEL-positive population contained a relevant fraction of cells where synapsis of the autosomes was not completed yet, i.e. zygotene and zygotene-like stage cells (Fig. 4A,B). Among them, the great majority were nuclei with an extension of synapsis that is typical of cells at early and mid-zygonema. This indicates that, in those nuclei, autosome synapsis was initiated but, just as it was observed in mutants with defects in recombination/synapsis of the autosomes, it could not be completed before reaching stage IV. We additionally analyzed the morphology of TUNEL-positive nuclei in *Mdc1*$^{-/-}$ mutant spermatocytes. In agreement with the observation that lack of *Mdc1* does not significantly impact autosomes synapsis (our observation and Ichijima et al., 2012), we observed that most cells in this mutant apoptose (at stage IV; Ahmed and de Rooij, 2009) after completing autosome synapsis (Fig. 4B). This led us to conclude that spermatocytes from *H2afx*$^{-/-}$ mice suffer from a defect in timely completion of autosome synapsis, as a result of a mechanism that does not involve *Mdc1*.

Lack of *H2afx* partially impairs the correct processing of DSBs

Building on the above findings, we hypothesized that *H2afx*$^{-/-}$ spermatocytes suffered from a defect in the processing of DSBs. In meiotic cells, repair of DSBs is characterized by the timely recruitment and release of several DSB-repair factors. Beside DMC1, these include MSH4 and MLH3 (e.g. Moens et al., 2002; La Volpe and Barchi, 2012). Quantification of DMC1 foci in late-zygonema cells of 12.5 dpp *H2afx* mutants revealed, by this stage, a rise in the number of foci. Moreover, the foci number was significantly higher, compared with the control, in (H1t-negative) early-pachynema nuclei (Fig. S4B, Table S1). This observation (that was confirmed in cells from adult mice, see below) suggests a delay in the processing of a subset of DSBs. One alternative interpretation is that the increase in the number of DMC1 foci may be caused by the occurrence of a late wave of SPO11-mediated DSBs. However, our observation that *H2afx* was dispensable to constrain SPO11 function, makes this hypothesis unlikely. To further understand whether the lack of *H2afx* might impact later recombination events, we quantified the MSH4 foci number. MSH4 is a member of the mammalian mismatch repair gene family, which binds onto recombination intermediates (i.e. Holliday junctions), and stabilizes homolog interaction, promoting synapsis (Kneitz et al., 2000; Snowden et al., 2004). In wild-type mice, foci of MSH4 appear first in early synapsed regions (i.e. synaptic forks) at early zygonema (Moens et al., 2007; Storlazzi et al., 2010). Subsequently, their number increases along synapsed cores at late zygonema, and a subset of foci persists until mid-pachynema (Santucci-Darmanin et al., 2000). We observed that, compared with wild-type cells, *H2afx*$^{-/-}$ spermatocytes displayed a small but significantly reduced number of foci at both zygotene and early-pachytene stages (Fig. 4C, Fig. S4C, Table S1). This difference was not just attributable to the variability of the genetic background of the animals, as it was consistently observed in a different set of mice with many – at least ten – generation gaps (Fig. S4D). We therefore concluded that lack of *H2afx* impacts on the proper assembly or stable

Journal of Cell Science (2018) 131, jcs214411. doi:10.1242/jcs.214411

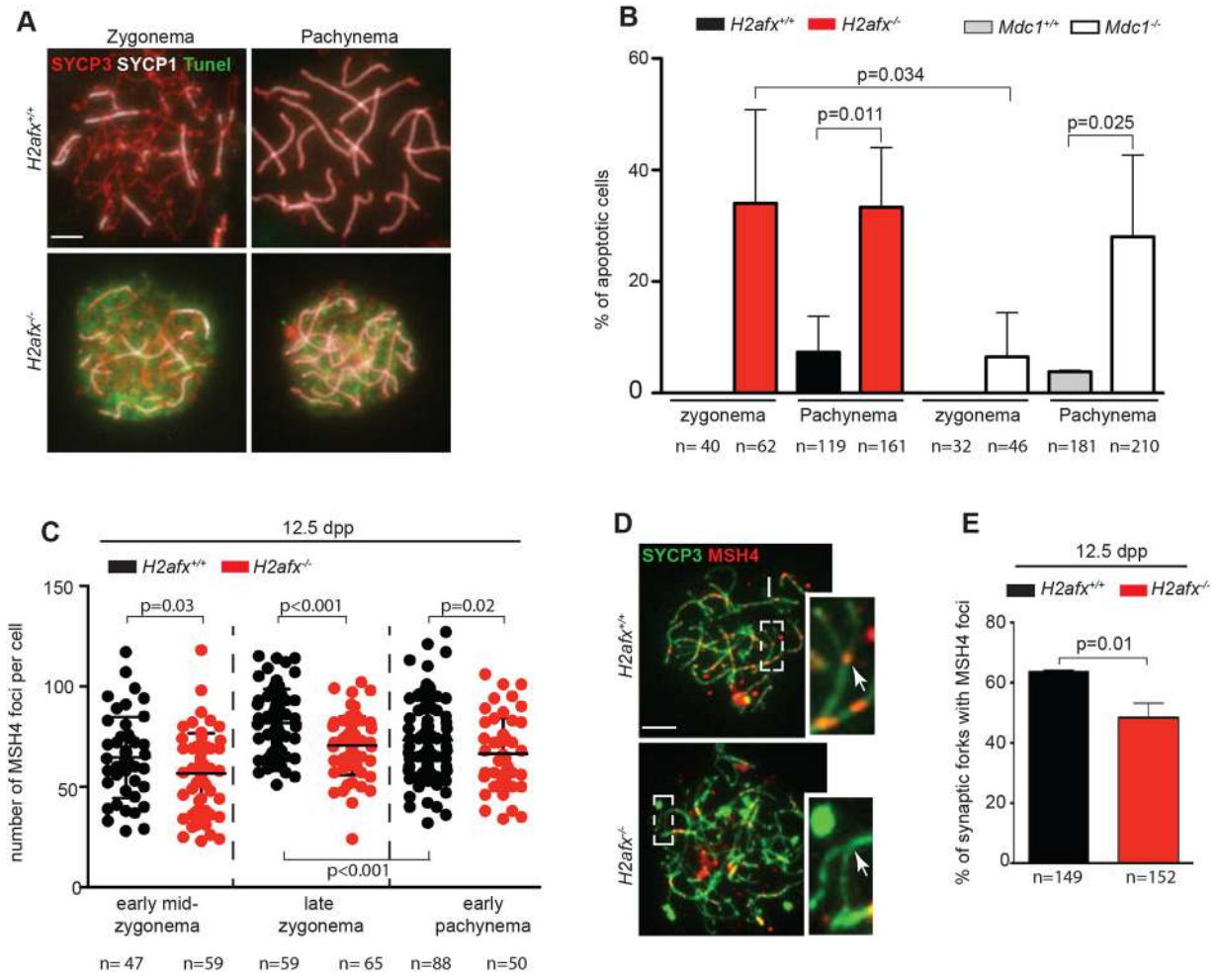

Fig. 4. A fraction of *H2afx*$^{-/-}$ spermatocytes dies by apoptosis before completion of autosomal synapsis and displays a defect in the assembly of MSH4 foci. (A) Representative images of nuclear spreads of *H2afx*$^{+/+}$ and *H2afx*$^{-/-}$ spermatocytes labeled with anti-SYCP3, anti-SYCP1 and TUNEL staining. (B) Quantification of apoptotic cells in chromosome spread preparations of the indicated genotypes (*n*=3 mice analyzed per genotype). (C) Quantification of MSH4 foci number in mice of the indicated genotypes. Each dot in the graph indicates the number of foci per nucleus (*n*=3 mice analyzed per genotype). (D) Representative images of nuclear spreads of indicated genotypes labeled with anti-SYCP3 and anti-MSH4 antibodies. Enlarged images are magnifications of dotted areas. The arrows indicate MSH4 foci at representative synaptic forks. Scale bars: 5 µm. (E) Quantification of MSH4 foci number in synaptic forks of spermatocytes of the indicated genotypes (*n*=2 mice analyzed per genotype). Data are mean±s.d.; *n*=number of cells analyzed.

binding of MSH4 foci onto chromosomes. Accordingly, we noticed that while the number of MSH4 foci declined significantly from late zygonema to early pachynema in wild-type cells, their number remained substantially unchanged in *H2afx*$^{-/-}$ spermatocytes (Fig. 4C, Table S1, Fig. S4D). This indicates that, when H2AFX is absent, the release of MSH4 from DNA is delayed, pointing to a reduced assembly of MSH4 as the underlying mechanism for the nucleus-wide reduction of foci number. To further strengthen this assumption, we quantified MSH4 fork-associated foci in both wild-type and *H2afx*$^{-/-}$ cells. We observed a reduction in MSH4 foci associated with synaptic forks in the mutant (Fig. 4D,E), which confirmed our hypothesis. Importantly, in *Mdc1*$^{-/-}$ spermatocytes, the number of MSH4 foci was similar to that of control (Table S1). This indicates that, unlike *H2afx*, *Mdc1* is dispensable for the assembly of MSH4 onto foci. Overall, our findings highlight that H2AFX is needed for proper processing of DSBs.

Both *H2afx* and *Mdc1* promote deposition of MLH3 foci at pachynema

It is known that in pachytene stage cells of *Mdc1*$^{-/-}$ and *H2afx*$^{-/-}$ spermatocytes, the assembly of MLH1 foci along the chromosome axes is severely reduced. This was suggested to be the consequence of the fact that, in these genotypes, spermatocytes die before MLH1 foci assembly begins (Ichijima et al., 2011; Celeste et al., 2002). However, an alternative interpretation is that when these genes are knocked out, the pro-crossover pathway is altered. To distinguish between these alternative interpretations, we stained wild-type, *H2afx*$^{-/-}$ and *Mdc1*$^{-/-}$ mice spermatocytes with an antibody that recognizes the mismatch-repair protein 3 (MLH3), a pro-crossover factor that appears at early pachynema, before the mutant cells undergo apoptosis at stage IV (Lipkin et al., 2002; Kolas et al., 2005; Svetlanov et al., 2008). Quantification of MLH3 foci in both genotypes revealed that, although MLH3 foci were present and increased significantly in number during the early pachynema (H1t-negative) to early mid-pachynema (faintly H1t-positive) transition, their global number was significantly smaller than that in the control (Fig. 5A–C). This indicates that *H2afx* and *Mdc1* are needed to promote the assembly or stable binding of MLH3 onto DNA. However, whether this phenotype is the consequence of either a delay or an arrest of the pro-crossover pathway in males, remains to be elucidated (see Discussion).

Journal of Cell Science (2018) 131, jcs214411. doi:10.1242/jcs.214411

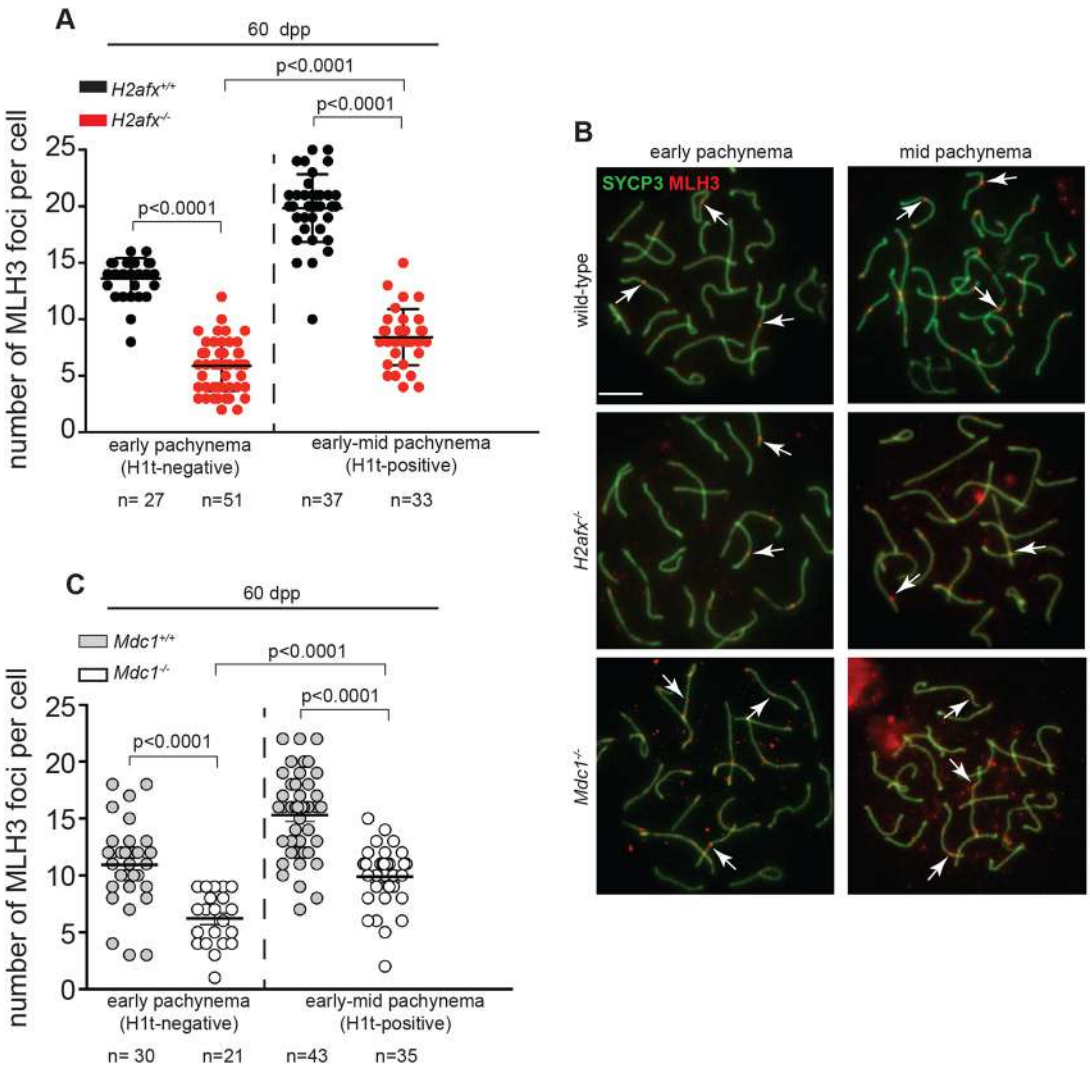

Fig. 5. *H2afx*$^{-/-}$ and *Mdc1*$^{-/-}$ spermatocytes are defective in MLH3 foci assembly. (A,C) Quantification of MLH3 foci in mice of the indicated genotypes and stages (*n*=3 mice analyzed per genotype). Each dot in the graph indicates the number of MLH3 foci per nucleus; data are mean±s.d.; *n*=number of cells analyzed. (B) Representative images of chromosome spreads from the indicated stages and genotypes, stained with anti-SYCP3 and anti-MLH3 antibodies. Arrows indicate MLH3 foci. Scale bar: 5 µm.

H2afx and *Mdc1* link resolution of DSBs with progression of spermatocytes to mid-pachynema

In mouse spermatocytes, mutations that lead to an increase in the number of DSBs at early pachynema or prevent DSBs from being repaired, cause a delay or arrest of spermatogenic differentiation following the activation of the recombination-dependent checkpoint (Pacheco et al., 2015; Crichton et al., 2017 preprint). Accordingly, in mutants, where the checkpoint is bypassed, normal coordination of progression with resolution of DSBs is altered, and cells enter mid-pachynema (i.e. incorporate the mid-pachytene stage marker H1t) though DNA damage persists. The activation of the checkpoint in mice, relies on the function of ATM (Pacheco et al., 2015). Since H2AFX is an ATM target (Rogakou et al., 1998; Barchi et al., 2008) and in somatic cells H2AFX phosphorylation is required to reinforce ATM signaling (Lou et al., 2006), we assumed that H2AFX might be involved in promoting activation of the recombination-dependent checkpoint. To determine whether lack of *H2afx* affects coordination between meiotic progression (i.e. incorporation of H1t) and repair of DSBs at pachynema, we used indirect immunofluorescence with antibodies against SYCP3, DMC1 and H1t on spermatocyte chromosome preparations. At first (as we had already observed in spermatocytes from juvenile mice), by analyzing the cells of the adult, we observed that H1t-negative pachytene spermatocytes showed higher numbers of DMC1 foci (Fig. 6A,BI,II). In addition, H1t-positive *H2afx*$^{-/-}$ spermatocytes also had numerous DMC1 foci, only ∼28% fewer than H1t-negative *H2afx*$^{-/-}$ cells (Fig. 6A,BII,IV). This was remarkably different from wild-type cells, where most of the cells that became H1t positive had a much lower number of DSBs (∼83% of reduction) than the early H1t-negative cells (Fig. 6A,BI,III). Moreover, H1t-positive *H2afx*$^{-/-}$ spermatocytes had significantly more DMC1 foci than H1t-positive wild-type cells (Fig. 6A, Fig. S4E). This suggests that, in the absence of *H2afx*, spermatocytes progress to mid-pachynema, despite the persistence of a high number of DSBs. Accordingly, as observed in other mice models with a defect in recombination-checkpoint activation (Pacheco et al., 2015), we found that in the mutant, the percentage of cells that progressed to mid pachynema was higher (wt, 35±5%; *H2afx*$^{-/-}$, 54±2%; $P<0.05$) (Fig. 7C). This phenotype is unlikely to be linked to alterations in the level or expression

Journal of Cell Science (2018) 131, jcs214411. doi:10.1242/jcs.214411

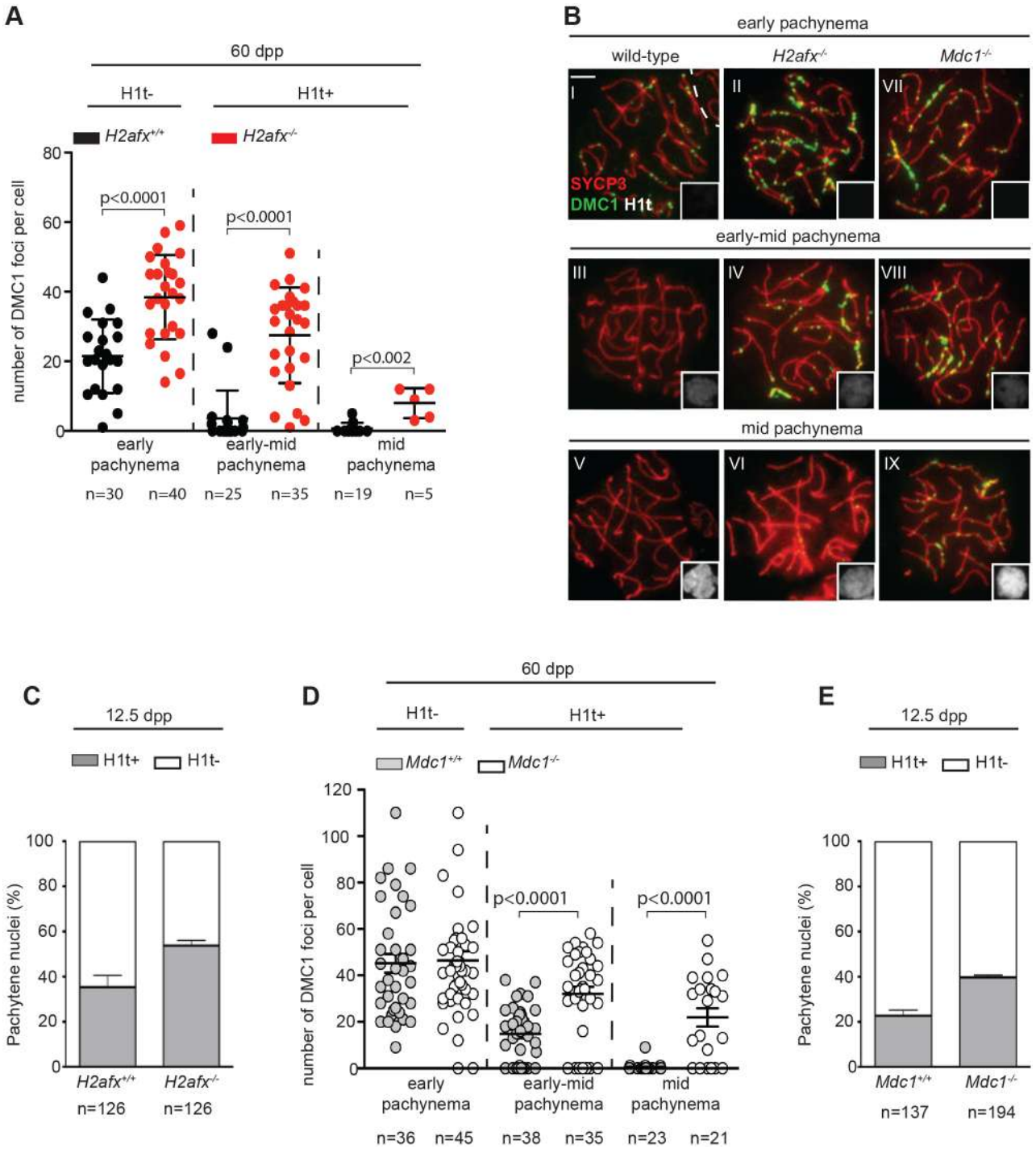

Fig. 6. *H2afx* and *Mdc1* genes tie DSBs repair with meiotic progression. (A,D) Quantification of DMC1 foci in mice of the indicated genotypes and stages (*n*=3 mice analyzed per genotype). Sub-classes of spermatocytes were identified by looking at the intensity of H1t staining (no staining=early pachynema; faint staining=early to mid-pachynema; intense staining=mid-pachynema). Each dot in the graph indicates the number of DMC1 foci per nucleus. (B) Representative images of nuclear spreads labeled with anti-SYCP3, anti-H1t (insert) and anti-DMC1, in cells with the indicated genotypes. Scale bar: 5 µm. (C,E) Percentage of H1t-positive spermatocytes from cells of the indicated genotypes. Data are mean±s.d.; *n*=number of analyzed cells.

timing of H1t, as those were found to be similar to that of controls (Fig. S5A–C). Hence, these observations indicate that *H2afx* mutant spermatocytes have a defect in coordinating repair of DSBs with meiotic progression. In order to understand whether *Mdc1* performs this function together with *H2afx*, we quantified the number of DMC1 foci in different sub-stages of pachynema in *Mdc1*$^{-/-}$ spermatocytes from adult mice. We observed that, at early pachynema, the average number of DMC1 foci was not different from that of control (Fig. 6D). Nevertheless, while the number of DSBs in cells that progressed to mid-pachynema was smaller by ∼70% in the wild type, the decrease was much lower (∼30%) in *Mdc1* mutant cells (Fig. 6BVII–IX, 6D). Since in *Mdc1*$^{-/-}$ spermatocytes the dynamics of DSB formation and repair were normal up to early pachynema, the observed increase in DMC1 foci in H1t-positive cells is unlikely to be due to a late wave of

Journal of Cell Science (2018) 131, jcs214411. doi:10.1242/jcs.214411

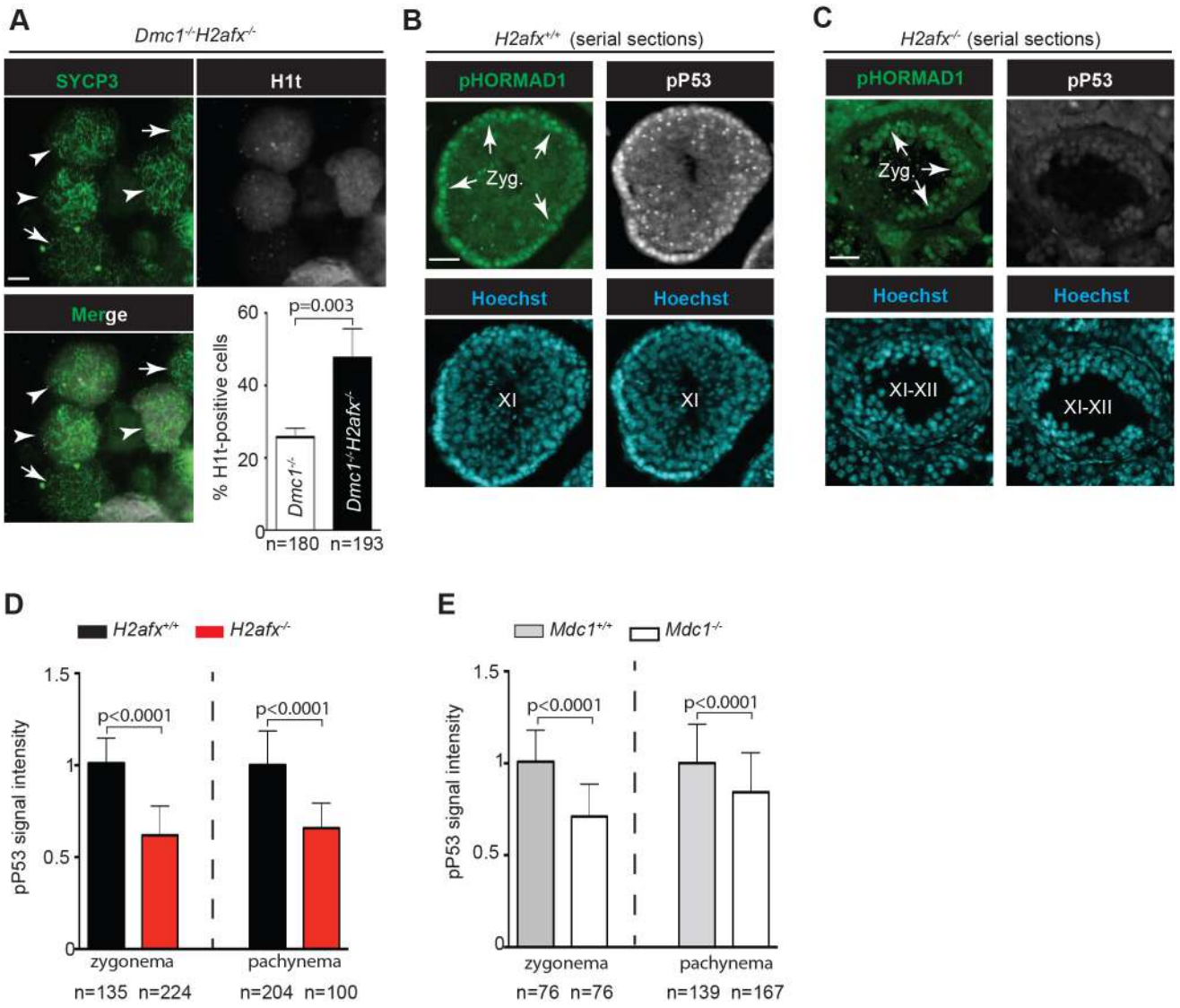

Fig. 7. *H2afx* supports activation of recombination-dependent arrest and P53. (A) Representative images and quantification of H1t-positive cells from the indicated genotypes (n=2 mice analyzed per genotype). Arrowheads indicate H1t-positive cells; arrows, H1t-negative nuclei. Scale bar: 5 µm. (B,C) Representative images of immunofluorescence staining of serial sections from testes of the indicated genotypes, stained with anti-pP53 and anti-pHORMAD1 antibodies. White arrows indicate spermatocytes at zygonema (Zyg.). Scale bars: 25 µm. Roman numbers indicate the stages of the epithelial cell cycle. (D,E). Quantification of pP53 signal in cells of the indicated stages and genotypes (n=3 mice analyzed per genotype). Data are mean±s.d., n=number of cells analyzed.

DSBs, or to a defect in DSB repair. Therefore, from this result we inferred that *Mdc1* is needed to impose a delay at early pachynema, which prevents premature progression to mid-pachynema. Accordingly, the count of H1t-positive cells in 12.5 dpp testes revealed that, in the mutant, the number of H1t-positive cells had increased (wt, 23±2%; *Mdc1*$^{-/-}$, 37%±1, P<0.05) (Fig. 6E), and in these H1t-positive cells, the number of DMC1 foci was higher relative to that in wild-type cells (Fig. S4F). Altogether, our observations suggested that, in mouse spermatocytes, *H2afx* and *Mdc1* are needed to link the resolution of DNA damage with meiotic progression through prophase I – a phenotype that indicates a defect in the activation of the recombination-dependent checkpoint (Pacheco et al., 2015; Crichton et al., 2017 preprint; Marcet-Ortega et al., 2017).

Dmc1$^{-/-}$ *H2afx*$^{-/-}$ spermatocytes progress to an H1t-positive state in greater numbers compared with *Dmc1*$^{-/-}$

To further challenge the hypothesis of a role for *H2afx* in constraining progression of spermatocytes with unrepaired damage, we sought to compare H1t incorporation in *Dmc1*$^{-/-}$ and *Dmc1*$^{-/-}$*H2afx*$^{-/-}$ double mutants. *Dmc1* deficiency prevents synapsis and DSB repair (Pittman et al., 1998) and spermatocytes were reported not to incorporate H1t (Barchi et al., 2005; Pacheco et al., 2015), or to incorporate it at low levels (Mahadevaiah et al., 2008). In line with previous results, using chromosome spread analyses, we observed that only a small portion of *Dmc1*$^{-/-}$ spermatocytes was faintly H1t-positive. This percentage increased significantly in *Dmc1*$^{-/-}$*H2afx*$^{-/-}$ double mutants (Fig. 7A) (*Dmc1*$^{-/-}$, 25.7±2%; *Dmc1*$^{-/-}$*H2afx*$^{-/-}$, 47.6±8%), which was suggestive of a less penetrant arrest or delay of progression in the double mutant. In spermatocytes, the incorporation of H1t is not prevented by a simple defect of chromosome synapsis (i.e. as if they lack *Spo11*; Barchi et al., 2005; Pacheco et al., 2015). Hence, our data represents a direct indication that *H2afx* supports the activation of a mechanism that constrains the meiotic progression of cells with unrepaired damage.

Journal of Cell Science (2018) 131, jcs214411. doi:10.1242/jcs.214411

Deletion of *H2afx* and *Mdc1* dampens P53-mediated activation to DSBs

In mouse spermatocytes, activation of the recombination-dependent arrest at pachynema relies on the function of P53 (Marcet-Ortega et al., 2017). We reasoned that, if *H2afx* and *Mdc1* are required to support the recombination-dependent arrest in spermatocytes, they might support P53 activation. In mouse, Spo11-mediated activation of P53 can be monitored by looking at its phosphorylation on Ser^{15} (pP53) (Lu et al., 2010). By immunostaining testes sections with the anti-pP53 antibody (using nuclear morphology and the anti-acrosin pattern for staging of seminiferous tubules; Muciaccia et al., 2013), we observed that the pP53 signal is present through prophase I from leptonema to pachynema as diffuse nuclear staining, while it became restricted to the X-Y chromosomes by mid/late pachynema (Fig. S6A,B). In those experiments, the pP53 signal was specific as it was absent in tissues and cell extracts from $p53^{-/-}$ mice (Fig. S7B). In somatic cells, P53 is a target of the ATM/Chk2 DNA-damage response pathway (Canman et al., 1998; Khanna et al., 1998; Banin et al., 1998). With a view to verifying whether, in spermatocytes, ATM and P53 are in the same pathway, we stained testes sections of $Atm^{-/-}$ mice with anti-γH2AFX and anti-pP53 antibodies. We focused on γH2AFX-negative cells at leptonema, because at that stage, the ATM function is not likely to be replaced by ATR (Bellani et al., 2005; Barchi et al., 2008; Royo et al., 2013). pP53 was not apparent in γH2AFX-negative nuclei (Fig. S7C), confirming that P53 is a target of ATM.

ATM signaling is canonically enhanced by a positive-feedback loop mechanism that involves MDC1 binding to γH2AFX (Yuan et al., 2010; Coster and Goldberg, 2010). Thus, to investigate whether both H2AFX and MDC1 are components of the ATM–P53 signaling cascade, we measured pP53 in both genotypes. We observed that the pP53 signal was dampened in pHORMAD1-positive zygonema cells, with a reduction of about 43% in $H2afx^{-/-}$ spermatocytes (Fig. 7B–D) and 30% in *Mdc1* mutant (Fig. 7E). Phosphorylation was also reduced at early to mid-pachynema to a similar extent in both mutants (Fig. 7D,E, Fig. S7D,E). Importantly, the weakening of the pP53 signal in mutant tissues was not due to a reduced expression of P53 as the protein was found to be present at similar levels in all genotypes (Fig. S7F). Considering the above, we concluded that, in spermatocytes, H2AFX and MDC1 support the activation of P53, in response to Spo11-mediated DSBs.

DISCUSSION

H2AFX enforces recombination-mediated synapsis of the autosomes

In somatic cells, besides fulfilling other functions, H2AFX and MDC1 promote the maintenance of genome stability by enforcing recombination-mediated DSB repair (Ünal et al., 2004; Xie et al., 2004; Sonoda et al., 2007; Bassing et al., 2002; Xie et al., 2007, 2010). In meiosis, whether *H2afx* plays a function in recombination-mediated synapsis is controversial (Moens et al., 2007; Mahadevaiah et al., 2008). In addition, whether the observed synaptic problem was due to a defect in DSB formation or to their correct processing, remained unknown. By analyzing DMC1 and BRCA1 deposition on bulk chromatin, we found that in the absence of *H2afx*, DSBs form in normal numbers. This is consistent with the observed normal levels of phosphorylation of HORMAD and SMC3 proteins (Fukuda et al., 2012). Nevertheless, we observed that chromosome dynamics were altered in a significant fraction of *H2afx* mutant cells at zygonema, thus suggesting that there was a recombination defect. In support of this hypothesis, we found that similar to mouse mutants where recombination is compromised (Barchi et al., 2005), a relevant fraction of cells that had not completed autosome synapsis died by apoptosis at stage IV of the epithelial cell cycle. This is the opposite of what we have recently observed in a mouse model with proficient recombination, where zygonema-like cells that receive a late surge of DSBs are able to complete chromosome synapsis timely (Faieta et al., 2016). This strengthens the hypothesis that *H2afx* is required to enforce recombination-mediated synapsis. In line with such a role, we demonstrated that the number of DMC1 foci had significantly increased in $H2afx^{-/-}$ cells at early pachynema (Fig. 8). In addition, the number of MSH4 foci was significantly lower at both zygotene and pachytene stages. The MutSγ complex, represented by MSH4 and MSH5, plays a well-established role in promoting homologous synapsis (Edelmann et al., 1999; Kneitz et al., 2000). From these observations, we inferred that H2AFX promotes synapsis of the autosomes, by enforcing recombination proficiency. As H2AFX is a histone, we assume that it might contribute to shape chromatin conformation and accessibility to DNA of repair factors, including MSH4 (Fig. 8). This hypothetical function may depend on the presence of H2AFX per se, or on the absence of some H2AFX post-translational modifications induced by DNA damage (Xie et al., 2010). However, since in somatic cells H2AFX-mediated function in recombination largely relies on its phosphorylation (Sonoda et al., 2007), we suppose that γH2AFX might be required to support meiotic recombination. This interpretation was corroborated by the observation that proper repair of DSBs in *Mdc1* mutant spermatocytes correlated with the presence of (albeit reduced) γH2AFX signal along chromosome axes (Lee et al., 2005). This interpretation is also consistent with the findings relating to somatic cells, where limited formation of γH2AFX, in the absence of *Atm*, is sufficient to support *H2afx*-dependent homologous recombination (Rass et al., 2013).

H2afx and *Mdc1* play partially overlapping functions in X-Y synapsis

Previous findings had shown that both $H2afx^{-/-}$ and $Mdc1^{-/-}$ spermatocytes suffered from a defect in X-Y chromosome synapsis (Fernandez-Capetillo et al., 2003; Celeste et al., 2003; Ichijima et al., 2011). However, the relative contribution of these genes to the process was not investigated. We observed that the percentage of X-Y asynapsis in $H2afx^{-/-}$ spermatocytes was threefold higher compared with that of $Mdc1^{-/-}$. This indicates that *H2afx* and *Mdc1* promote sex chromosome synapsis through mechanisms that are at least partially distinct. The above observations on synapsis and recombination of the autosomes suggest that sex chromosome asynapsis in *H2afx* spermatocytes is due to the reduced proficiency of recombination, which was not observed in mutants lacking *Mdc1*. A common feature of *H2afx* and *Mdc1* mutant spermatocytes is the lack of formation of the sex body, a chromatin domain that promotes X-Y proximity, and it is thought to assist recombination-mediated synapsis at the PAR (Fernandez-Capetillo et al., 2003; Celeste et al., 2003; Ichijima et al., 2011; Kauppi et al., 2011). Therefore, a reasonable interpretation is that X-Y asynapsis in the *Mdc1* mutant is due to a reduced chance of sex chromosomes to be spatially close at the late zygonema to early pachynema transition, the time at which X-Y recombination occurs in normal mice (Kauppi et al., 2011). In *H2afx* mutant spermatocytes, the defect in the formation of the sex body would be additional to that of recombination, resulting in a greater frequency of asynapsis. Therefore, we concluded that in mice, efficient synapsis of the sex chromosomes depends on both *H2afx* and *Mdc1*, although with only partially overlapping mechanisms.

Journal of Cell Science (2018) 131, jcs214411. doi:10.1242/jcs.214411

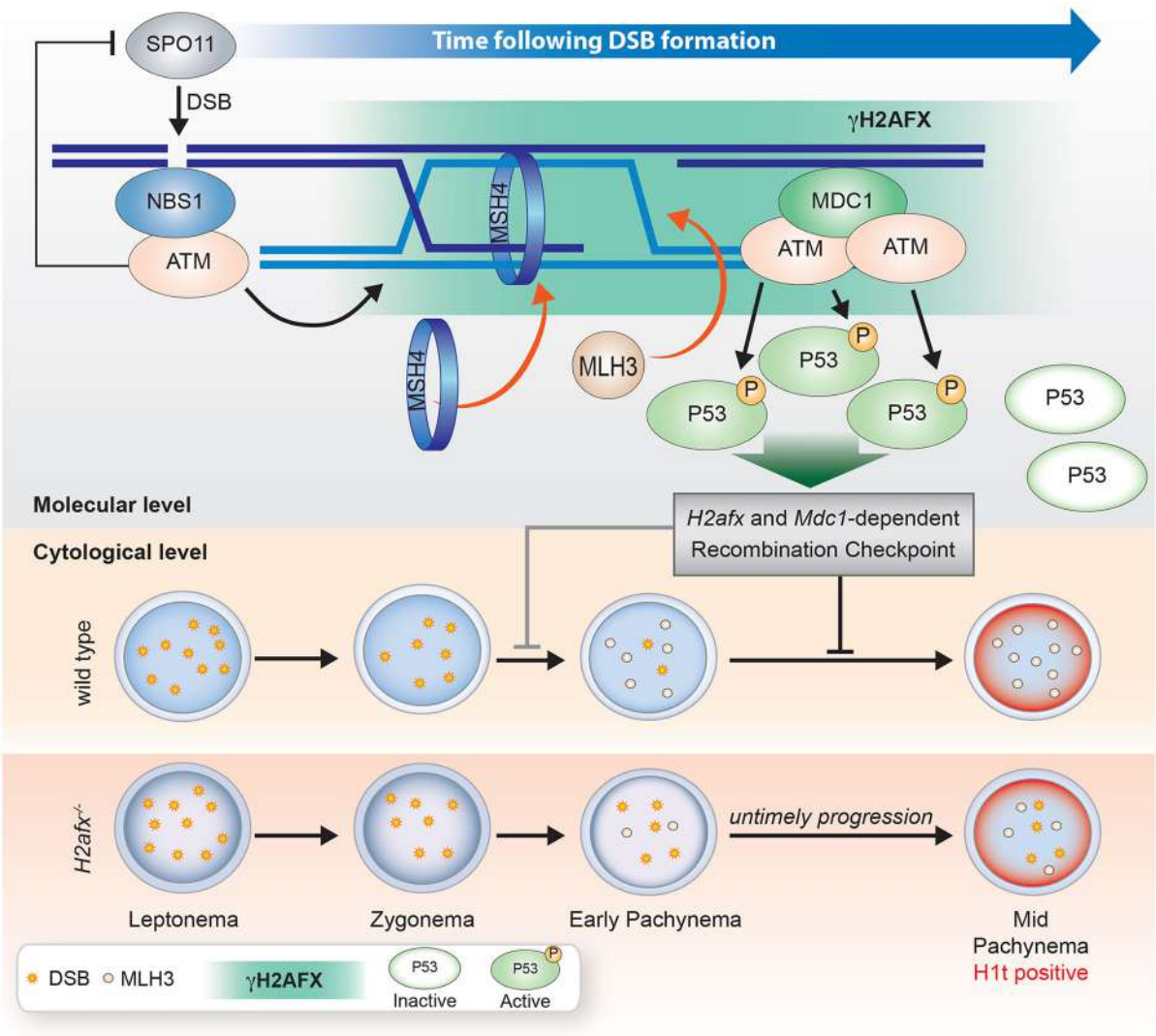

Fig. 8. Schematic model showing H2AFX and MDC1 functions in response to Spo11-mediated DSBs in spermatocytes. Based on the information presented in this and previous studies, we propose the following model. Once ATM is activated by SPO11-induced damage, SPO11 catalytic activity is inhibited (Lange et al., 2011) by a mechanism that does not require *H2afx* or *Mdc1* (thin black line, top). Following the phosphorylation of H2AFX (γH2AFX) by ATM, chromatin conformation might be modified to assist proper recruitment of MSH4 at zygonema and recruitment/stabilization of MLH3 at early pachynema (top and wild-type panel). This would support stable alignment and pairing of the homologs (not shown). In the wild type, proper control of meiotic progression requires robust ATM–H2AFX–MDC1-mediated activation of P53. The latter activates the recombination-dependent checkpoint that partially constrains progression of cells at zygonema (light gray line), and prevents untimely progression to mid pachynema (black line). In the absence of *H2afx* (or *Mdc1*, not shown), MLH3 assembly/stabilization onto chromosomes is delayed. Moreover, the activation of P53 is dampened, and damaged cells at early pachynema progress to mid-pachynema (*H2afx*$^{-/-}$). DSB, double-strand break.

H2AFX and MDC1 promote the timely execution of the pro-crossover pathway

In normal cells, out of about 200–300 DSBs that form during early prophase of meiosis I in mouse spermatocytes, only a small subset go on to become COs (~20–30). Designation of prospective COs is implemented gradually during meiosis (Cole et al., 2012) by a mechanism that requires the assembly of recombination factors that include MSH4 and MLH3 (Kolas et al., 2005). In our analyses, we observed that the number of MLH3 foci at pachynema was significantly reduced in *Mdc1*$^{-/-}$ and *H2afx*$^{-/-}$ spermatocytes (Fig. 8). This indicates an alteration of the pro-crossover pathway. However, MSH4 foci were not reduced in the absence of *Mdc1*. This indicates that the reduction of MSH4 we observed in *H2afx*$^{-/-}$ cells was not likely to be mechanistically linked to that of MLH3. It is thus conceivable that *H2afx* and *Mdc1* genes, by contributing to properly shape chromatin, might promote CO formation, perhaps stabilizing MLH3 binding onto DNA, or by favoring the interaction of DNA with CO designation factors (such as ZMM proteins other than MSH4; Lynn et al., 2007; Adelman and Petrini, 2008; Reynolds et al., 2013), that assemble onto chromosomes prior to MLH3. MDC1 may serve, per se, as a scaffold for the recruitment of such factors. Alternatively, as H2AFX is partially phosphorylated in *Mdc1*$^{-/-}$ cells, correct MLH3 deposition might require robust levels of (MDC1-mediated) γH2AFX.

Evidence against a mechanistic role of *H2afx* and *Mdc1* in CO formation is that, in females, MLH1 foci assemble normally (Celeste et al., 2002; Ichijima et al., 2011). This might depend on the different timing of the arrest of defective oocytes. In females, the DNA damage-independent and -dependent arrests only act in oocytes at late prophase (Bolcun-Filas et al., 2014; Cloutier et al.,

Journal of Cell Science (2018) 131, jcs214411. doi:10.1242/jcs.214411

2015). Given that, a possible explanation for the apparent sexual dimorphism in MLH3/MLH1 foci assembly in *H2afx* and *Mdc1* mutants is that CO designation is delayed in both sexes rather than being arrested. This would allow oocytes from *H2afx* mice to complete synapsis and place (in both $H2afx^{-/-}$ and $Mdc1^{-/-}$ genetic backgrounds) MLH3 (and MLH1) at CO sites, with no consequent overt defect in female fertility. Accordingly, we observed that in males, the average number of MLH3 foci increased through the early pachynema to mid-pachynema transition, although they were less numerous compared with the control. This indicates that MLH3 foci continued to be deposited over time, with slow kinetics, before their apoptotic elimination at stage IV of the epithelial cell cycle.

Arrest of progression before H1t incorporation at pachynema depends on levels of γH2AFX and pP53

In recombination-defective mutants, persistent unrepaired DSBs at pachynema are marked by γH2AFX. The progression of those cells through differentiation correlates with the lack or low levels of γH2AFX along autosomes axes, such as in the *Trip13* mutant (Pacheco et al., 2015). Based on this observation, we argued that in spermatocytes, γH2AFX might represent a signal to constrain cell progression through differentiation. In line with this hypothesis, we observed that in $H2afx^{-/-}$ mice, the percentage of H1t-positive cells at pachynema was significantly higher compared with the wild type. Moreover, the number of DSBs in H1t-positive mutant cells was also significantly higher compared with that in the control. Hence (as observed for other proteins involved in the ATM signaling pathway; Pacheco et al., 2015) H2AFX is likely required to implement coordination of DSB repair with meiotic progression. Likewise, although *Mdc1* is dispensable for timely repair of DSBs, the percentage of H1t-positive cells in the mutant was higher than that in the wild-type, and H1t-positive $Mdc1^{-/-}$ spermatocytes displayed a significantly higher number of unrepaired DSBs compared with its control. This is the first demonstration that, in recombination-proficient cells, the recombination-dependent arrest prevents premature early-pachynema to mid-pachynema transition. In $Mdc1^{-/-}$ spermatocytes, H2AFX is phosphorylated at low levels during meiosis (Lee et al., 2005). Therefore, bypass of recombination-dependent arrest would reflect the persistence of γH2AFX below a threshold level.

In somatic cells, MDC1-mediated phosphorylation of H2AFX amplifies the ATM response to damage. The latter promotes either the arrest of the cell cycle, or apoptosis (Stewart et al., 2003). ATM effectors on these functions include P53, which has been recently implicated in the activation of the recombination-dependent checkpoint in male meiosis (Pacheco et al., 2015; Marcet-Ortega et al., 2017). We observed that impaired co-ordination of meiotic progression and DSB repair in $H2afx^{-/-}$ and $Mdc1^{-/-}$ cells at pachynema correlate with an obvious reduction of pP53 in the nucleus. Therefore, according to what is known in somatic cells, we suggest that in mouse meiosis, arrest of differentiation by the recombination-surveillance mechanism depends on the persistence, at pachynema, of a (MDC1-mediated) sufficiently high γH2AFX signal. The latter, by amplifying the ATM responses, would implement the activation of P53 (Fig. 8), delaying or arresting the progression as long as a sufficient number of DSBs has been repaired, and the drop of γH2AFX and pP53 below a threshold level.

An additional aspect of mouse meiotic cell response to SPO11-mediated DSB formation is the inhibition, by the ATM and MRE11 complex, of SPO11 activity (Lange et al., 2011; Pacheco et al., 2015) (Fig. 8). In somatic cells, the interaction of the MRE11 complex with DSBs promotes the recruitment of ATM onto damaged DNA before the appearance of γH2AFX. Further accumulation of the ATM and MRE11 complex around DSB sites occurs by a mechanism that requires (MDC1-mediated) H2AFX phosphorylation. Therefore, ATM and MRE11 complex-mediated control over the number of DSBs might occur either before or after phosphorylation of H2AFX. Our finding that the number of DSBs is unaltered in both $H2afx^{-/-}$ and $Mdc1^{-/-}$ cells, suggests that γH2AFX is dispensable to exert a control over SPO11 activity. Hence, while both the control of the number of DSBs and the activation of recombination-dependent checkpoint depend on ATM, only the latter additionally requires amplification of ATM signaling, through the functions of H2AFX and MDC1 (Fig. 8).

H2afx plays a minor function in the arrest of progression of zygonema cells with irreparable DSBs

In mice carrying deletion of *Dmc1*, chromosome synapsis and recombination are impaired, and no or few cells progress and incorporate H1t. Conversely, in cells where DSB formation is prevented (i.e. $Spo11^{-/-}$ mutant), despite defective synapsis, H1t deposition occurs efficiently (Barchi et al., 2005). This indicates that the mechanism that prevents the cytological progression of zygotene stage cells to mid-pachynema, depends on the persistence of unrepaired DSBs. The genes responsible for the activation of such recombination-dependent arrest are unknown. Our observation that in a $Dmc1^{-/-}$ background, the lack of *H2afx* partially releases the arrest of progression of cells with persistent damage, points to a role for *H2afx* in this mechanism. However, in this genetic contest, the contribution of *H2afx* is mild, as in $Dmc1^{-/-}H2afx^{-/-}$ mutants we observed only a modest increase in the number of H1t-positive cells relative to that in $Dmc1^{-/-}$. In addition, the H1t staining in cells of the double mutants was as faint as that of the single mutant (Fig. S6C). This is likely to happen because of the persistence of a massive load of irreparable DSBs. In *Caenorhabditis elegans*, the damage-dependent apoptosis in the germ line requires *msh4* and *msh5* (Silva et al., 2013). In mouse, albeit *Msh5* deletion prevents DSB repair in spermatocytes, cells incorporate H1t prior to their elimination at stage IV (Barchi et al., 2005). This makes *Msh5* an ideal (not yet tested) candidate gene to be involved in the recombination-mediated arrest at zygonema. Therefore, the full understanding of the mechanisms underlying the control of meiotic progression continues to be a challenge for the future.

MATERIALS AND METHODS

Mice and genotyping

H2afx, *Mdc1*, *Dmc1*, *p53* and *Atm* mutant mice were on a C57BL6×129 S/v mixed background. To minimize variability from strain background, experimental animals were compared with controls from the same litter or from the same mating involving closely related parents. Each analysis was done with 2 to 4 animals per genotype. No significant variations were observed between individual or between litter comparisons of animals with the same genotype. $H2afx^{-/-}$ and $Mdc1^{-/-}$ mice were generated from $H2afx^{+/-}$ and $Mdc1^{+/-}$ intercrosses, respectively. $H2afx^{-/-}Dmc1^{-/-}$ males were generated by crossing $H2afx^{+/-}$ with $Dmc1^{+/-}$ mice. The genotyping of *H2afx*, *Mdc1*, *Dmc1* and *Atm* was performed by PCR of tail tip DNA. Primer sequences are reported elsewhere (Celeste et al., 2002; Lou et al., 2006; Pittman et al., 1998; Barchi et al., 2008). Tissue samples from $p53^{-/-}$ mice were provided by Dr Travis Stracker (IRB, Barcelona, Spain); mouse embryonic fibroblasts (MEFs) were a gift from Dr Fabiola Moretti (CNR, Rome, Italy).

Preparation of meiotic chromosome spreads

Spreads of germ cell chromosomes were performed according to Faieta et al. (2016). In brief, testes were removed from euthanized animals, decapsulated,

Journal of Cell Science (2018) 131, jcs214411. doi:10.1242/jcs.214411

chopped in high-glucose MEM and mixed. Suspension was left to settle down and the supernatant was spun down at 7200 rpm for 1 min. The pellet was resuspended in 0.5 M sucrose and the suspension was added to slides coated with 1% paraformaldehyde in 0.015% Triton X-100, and incubated for 2 h in a humidified chamber at room temperature (RT). At the end of the incubation, slides were rinsed twice in 1:250 Photo-flo Kodak professional (no. 1464510) in water and allowed to air dry. Surface chromosome spreads were either immediately processed for immunofluorescence or stored at −80°C for up to 6 months.

Immunofluorescence assay and quantification of fluorescence intensity

After 10 min washes with washing buffer 1 (0.4% Photo-flo, 0.01% Triton X-100 in water), surface spreads were incubated overnight at room temperature with the primary antibody in antibody dilution buffer (ADB) [10% goat serum, 3% bovine serum albumin (BSA), 0.05% Triton X-100 in phosphate-buffered saline (PBS)]. After one wash in washing buffer 1, and one in washing buffer 2 (0.4% Kodak Photo-flo in water) for 10 min each, slides were incubated with the secondary antibody for 1 h in a pre-warmed humidified chamber at 37°C in the dark. After 10 min washes with washing buffers 1 and 2, slides were rinsed for 5 min in PBS and incubated in Hoechst 33258 in PBS for at least 15 min in a humidified chamber, at RT. At the end of the incubation, slides were air-dried for 10 min at RT in the dark, and mounted using ProLong Gold Antifade Mountant without DAPI (Molecular Probes, Life Technologies cat. no. P36934). Images were captured using Leica CTR6000 Digital Inverted Microscope connected to a charge-coupled device camera and analyzed using the Leica software LAS-AF for fluorescent microscopy.

Sources and dilutions of antibodies for immunofluorescence were as follows: mouse anti-SYCP3 (Santa Cruz Biotechnology, sc-74569) 1:300; rabbit anti-SYCP3 (Novus Biologicals, nb300-231) 1:300; rabbit anti-SYCP1 (Abcam, ab15090) 1:200; rabbit anti-DMC1 (Santa Cruz, sc 22768) 1:100; rabbit anti-γH2AX (Cell Signaling, 9718) 1:400-500; guinea pig anti-H1T (a gift from M. A. Handel, The Jackson Laboratory, Bar Harbor, ME, USA) 1:500; rabbit anti-pHORMAD1 s375 (a gift from C. Hoog, Karolinska Institute, Stockholm, Sweden) 1:200; rabbit anti-HORMAD2 (a gift from A. Toth, TU Dresden, Dresden, Germany) and rabbit anti-MLH3 (a gift from P. Cohen, Cornell University College of Veterinary Medicine, Ithaca, NY, USA) 1:100; rabbit anti-MSH4 (Abcam, ab58666) 1:75; rabbit anti-pP53 Ser^{15} (Cell Signaling, 9284) 1:100; monoclonal mouse anti-human Acrosin (AMC-ACRO-C5F10-AS) 1:200; rabbit anti-BRCA1 (a gift from Satoshi Namekawa, Cincinnati Children's Hospital Medical Center, Cincinnati, OH, USA) 1:1000) 1:200. Alexa Fluor-conjugated secondary antibodies (Molecular Probes, Life Technologies) were diluted 1:200.

The intensity of H1t and pP53 signals were measured using the LAS-AF software (Leica). Measures were performed by choosing a fixed-size region of interest, which included most of the diameter of the nucleus. Measurements were performed only on nuclei of approximately the same size. For H1t measurements, we considered positive, all cells with a signal above the background signal measured in pre-leptonema/leptonema nuclei.

Terminal deoxynucleotidyl transferase dUTP nick end labeling (TUNEL)

TUNEL assay was performed after immunofluorescence, according to Pacheco et al. (2015), using the In Situ Cell Death Detection Kit (POD) from Roche (cat. no. 11684817910).

Preparation of clone DNA by alkaline lysis and nick translation

BAC clones for Y chromosome (RP24 502P5), X chromosome (RP25 470D15) and PAR region (RP24500I4) were grown in standard Luria Bertani medium at 32°C for a minimum of 16 h. Purification of DNA, after overnight culture, was obtained with Plasmid Maxi Prep Kit (Qiagen). The determination of DNA concentration was made by both UV spectrophotometry at 260 nm and quantitative analysis on agarose gel. Approximately 1 µg of extracted BAC DNA was marked with fluorescent isotopes using Nick Translation Kit (Abbott Molecular) according to the manufacturer's instructions. Probe sizes were determined with a quantitative analysis of agarose gel. All probes were combined with *in situ* hybridization buffer (Enzo Life Sciences) according to the manufacturer's instructions in the presence of 0.1 µg/µl mouse Cot-1 DNA (Invitrogen). Probes were denatured at 73°C for 5 min in a water bath.

Fluorescence *in situ* hybridization (FISH) of the PAR

Following immunofluorescence, slides with nuclear spreads were washed with fresh PBS at RT for 5 min, rinsed briefly in dH_2O, then dehydrated passing through an ethanol series and air-dried. After aging (65°C for 1 h), slides were denatured for 7 min in 70% formamide/2× SSC solution at 72°C and immediately dehydrated, passing it through ethanol series at −20°C, and air-dried. The FISH probe was applied to the slides and allowed to denature in a humid chamber at 75°C for 10 min. Hybridization was performed in a humid chamber at 37°C for a minimum of 16 h. Following two washes with stringent wash buffer (4× SSC/0.2% Tween-20) at 55°C, slides were dehydrated through an ethanol series and air-dried. Nuclei were stained with Hoechst 33258 for 20 min at RT. Aliquots of antifade solution were applied on the slides. Images were captured using Leica CTR6000 digital inverted microscope.

RNA extraction and RT-PCR

Testes from 10.5 and 12.5 dpp $H2afx^{-/-}$ and $H2afx^{+/+}$ mice were dissected and homogenized in 500 µl of QIAzol Lysis Reagent (cat. no. 79306). RNA extraction was performed according to the manufacturer's instructions and diluted in DEPC water. Contaminating genome DNA was removed with a DNA-free kit (Ambion, AM1906). Synthesis of cDNA was performed with Invitrogen RT-PCR SuperScript III (Invitrogen, 18080-051) according to the manufacturer's instructions. SPO11 splice isoforms were amplified by PCR using 2 µl cDNA. Primer sequences are listed in Table S2.

Histological analysis of the testis

For histological analysis, testes were collected and fixed overnight at 4°C in Bouin's fixative (Sigma, HT10132). Freshly collected samples were weighed before fixation. Fixed samples were embedded in paraffin. Sections of 5 µm were stained with periodic acid–Schiff/hematoxylin (PAS) (Schiff's fuchsin-sulfite reagent, Sigma S5133). Images were captured using a Zeiss Axioskop bright-field microscope equipped with a color CCD camera.

Immunofluorescence analysis of the testis

Testes were removed from euthanized $H2afx^{+/+}$, $H2afx^{-/-}$, $Mdc1^{+/+}$, $Mdc1^{-/-}$, $P53^{+/+}$, $P53^{-/-}$ and $Atm^{-/-}$ adult animals and placed in at least 10 volumes of 4% paraformaldehyde in PBS, overnight at 4°C. The following day, tissues were immediately embedded in paraffin blocks, as per standard protocol. For immunofluorescence analyses, paraffin-embedded testes were sectioned at 3–5 µm. Following deparaffinization and rehydration, sections were treated to unmask the antigenic epitope, using Tris-EDTA citrate buffer, pH 7.8 (UCS diagnostic, TECH199). Sections were then rinsed in dH2O to continue with immunofluorescence (see above).

Preparation of testis nuclear extracts

The procedures for the preparation of the insoluble fraction of testis nuclear extracts, and antibodies sources for the detection of the phosphorylation status of HORMAD1, HORMAD2, SYCP2, STAG3, REC8, SMC3, in $H2afx^{+/+}$ and $H2afx^{-/-}$ mice are described elsewhere (Fukuda et al., 2012).

Immunoprecipitation and western blot

Immunoprecipitation and detection of pS1083 of SMC3 were performed as described in Fukuda et al. (2012). Immunoprecipitation of SPO11 was performed using a previously described technique (Neale et al., 2005; Lange et al., 2011). In brief, testes from 12.5 dpp $H2afx^{-/-}$, $H2afx^{+/+}$, $Dmc1^{+/+}$, $Dmc1^{-/-}$, $Spo11^{+/+}$ and $Spo11^{-/-}$ mice were decapsulated and lysed in lysis buffer (1% Triton X-100, 400 mM NaCl, 25 mM HEPES-NaOH at pH 7.4, 5 mM EDTA). Lysates were subjected to two rounds of centrifugation at 13,200 rpm for 15 min each at 4°C in a benchtop centrifuge. Supernatants were incubated with monoclonal mouse anti-SPO11 antibody 180 (3 µg per pair of testes) at 4°C for 1 h, followed by the addition of 40 µl Protein-A agarose beads (Roche) and incubated for an additional 3 h at 4°C. After incubation, beads were washed three times with IP buffer (1% Triton X-100, 150 mM NaCl, 15 mM Tris-HCl at pH 8.0, 1 mM EDTA).

Immunoprecipitates were eluted with Laemmli sample buffer. Samples were fractionated on 8% SDS-PAGE and transferred to a PVDF membrane by the semi-dry transfer system (Bio-Rad). For western analysis, membranes were probed with antibody anti-mSPO11 antibody 180 (1:2000 in PBS containing 0.1% Tween 20 and 5% non-fat dry milk) overnight at 4°C and then with horseradish peroxidase-conjugated protein A (Abcam; 1:10,000 in PBS containing 0.1% Tween 20 and 5% non-fat dry milk) for 2 h at room temperature. Signals were detected using the ECL+ reagent (GE Healthcare). Western blotting of P53, pP53 and CHK2 were performed as described above with some modifications: testes samples collected from 10.5 dpp mice, and MEF, were lysed in RIPA lysis buffer (100 mM NaCl, 10 mM $MgCl_2$, 30 mM Tris-HCl, 0.5% Triton X-100) with the addition of 1 mM DTT, 0.5 mM sodium orthovanadate and protease inhibitors (Roche). MEFs were treated with 10 µM bleomycin for 4 h. Sources and dilutions of antibodies were as follows: anti-P53 antibody (DB-Biotech, no. 002) 1:2000 in TBST 5% milk (ChemCruz); anti-pP53 antibody (Cell Signaling, 9284) 1:1000 in 5% milk; anti-CHK2 antibody (Millipore, 05-649) 1:500 in 5% BSA, TBST (Tris buffered saline, 0.1% Tween 20).

Detection of SPO11–oligonucleotide complexes

SPO11–oligonucleotide complexes were analyzed as described in Neale et al. (2005) and Lange et al. (2011). In short, following two rounds of immunoprecipitation with an anti-SPO11 monoclonal antibody (Spo11-180), SPO11-oligonucleotide complexes were labeled with [α-^{32}P]dCTP, using terminal deoxynucleotidyl transferase (TdT), and subsequently released from the beads, by boiling in Laemmli buffer. Samples were fractionated by SDS-PAGE, and the electrophoresed products were transferred onto a PVDF membrane. Radiolabeled species were detected using Fuji phosphor screens and analyzed with ImageGauge software. To identify SPO11 protein, the same PVDF membrane was subjected to western analysis, using the SPO11 monoclonal antibody and Protein-A–HRP secondary antibody, as described above.

Statistical analysis

Statistical analysis was performed using GraphPad Prism 5 for Macintosh (GraphPad Software, San Diego, CA). Data were expressed as mean±s.d. The statistical significance of data expressed in percentages was analyzed using Student's *t*-test after arcsin transformation of the data ($P<0.05$). Statistical significance of all other data regarding the comparison of foci numbers among different genotypes was analyzed by using the Mann–Whitney test ($P<0.05$).

Ethics statement

All applicable international, national and/or institutional guidelines for care and use of animals were followed. Mice work was approved by the animal health committee of the University of Rome Tor Vergata, and by the Ministry of Health of Italy. This article does not contain any studies with human participants performed by any of the authors.

Acknowledgements

We thank P. Cohen (Cornell University), M. A. Handel (The Jackson Laboratory), C. Höög (Karolinska Institute), A. Toth (TU Dresden) and S. Namekawa (University of Cincinnati) for the generous gift of antibodies. We are also grateful to A. Nussenzweig (NIH) for providing *H2afx*$^{+/-}$ mice; J. C. Schimenti (Cornell University) for the *Dmc1*$^{+/-}$ mice; Scott Keeney and Maria Jasin (MSKCC) for the *Spo11*$^{-/-}$ mice; Sott Keeney and Julian Lange (MSKCC) for their help with the SPO11-oligo assay; Travis Stracker (IRB, Barcelona) and Fabiola Moretti (CNR, Italy) for providing us tissues and cells from *p53*$^{-/-}$ mice.

Competing interests

The authors declare no competing or financial interests.

Author contributions

Conceptualization: E.T., M.B.; Methodology: S.D.C., E.B., M.D.G., M.B.; Validation: E.T., D.N., C.A., M.F., S.D.C.; Formal analysis: E.T., D.N., C.A., M.F., S.D.C., T.F., M.B.; Investigation: E.T., D.N., C.A., M.F., C.C., T.F., M.B.; Resources: L.Z., A.M., I.R.; Data curation: E.T., D.N., C.A., M.F., M.D.G., M.B.; Writing - original draft: E.T., M.B.; Writing - review & editing: E.T.; Visualization: M.D.G.; Supervision: M.B.; Project administration: M.B.; Funding acquisition: M.B.

Funding

This work was supported by Fondazione Telethon Grant [GGP12189 to M.B. and Claudio Sette], PRIN 2010 from Ministero Italiano dell'Università e della Ricerca Scientifica [2010M4NEFY_004 to M.B.] and Mission Sustainability grant [ID 141 to M.B.] from the Università degli Studi di Roma Tor Vergata. The funders had no role in the study design, data collection and analysis, decision to publish, or preparation of the manuscript.

Supplementary information

Supplementary information available online at
http://jcs.biologists.org/lookup/doi/10.1242/jcs.214411.supplemental

References

Adelman, C. A. and Petrini, J. H. J. (2008). ZIP4H (TEX11) deficiency in the mouse impairs meiotic double strand break repair and the regulation of crossing over. *PLoS Genet.* **4**, e1000042.

Ahmed, E. A. and de Rooij, D. G. (2009). Staging of mouse seminiferous tubule cross-sections. *Methods Mol. Biol.* **558**, 263-277.

Banin, S., Moyal, L., Shieh, S. Y., Taya, Y., Anderson, C. W., Chessa, L., Smorodinsky, N. I., Prives, C., Reiss, Y., Shiloh, Y. et al. (1998). Enhanced phosphorylation of p53 by ATM in response to DNA damage. *Science* **281**, 1674-1677.

Barchi, M., Mahadevaiah, S., di Giacomo, M., Baudat, F., de Rooij, D. G., Burgoyne, P. S., Jasin, M. and Keeney, S. (2005). Surveillance of different recombination defects in mouse spermatocytes yields distinct responses despite elimination at an identical developmental stage. *Mol. Cell. Biol.* **25**, 7203-7215.

Barchi, M., Roig, I., di Giacomo, M., de Rooij, D. G., Keeney, S. and Jasin, M. (2008). ATM promotes the obligate XY crossover and both crossover control and chromosome axis integrity on autosomes. *PLoS Genet.* **4**, e1000076.

Bassing, C. H., Chua, K. F., Sekiguchi, J., Suh, H., Whitlow, S. R., Fleming, J. C., Monroe, B. C., Ciccone, D. N., Yan, C., Vlasakova, K. et al. (2002). Increased ionizing radiation sensitivity and genomic instability in the absence of histone H2AX. *Proc. Natl. Acad. Sci. USA* **99**, 8173-8178.

Bellani, M. A., Romanienko, P. J., Cairatti, D. A. and Camerini-Otero, R. D. (2005). SPO11 is required for sex-body formation, and Spo11 heterozygosity rescues the prophase arrest of Atm–/– spermatocytes. *J. Cell Sci.* **118**, 3233-3245.

Bishop, D. K., Park, D., Xu, L. and Kleckner, N. (1992). DMC1: a meiosis-specific yeast homolog of E. coli recA required for recombination, synaptonemal complex formation, and cell cycle progression. *Cell* **69**, 439-456.

Bolcun-Filas, E. and Schimenti, J. C. (2012). Genetics of meiosis and recombination in mice. *Int. Rev. Cell Mol. Biol.* **298**, 179-227.

Bolcun-Filas, E., Rinaldi, V. D., White, M. E. and Schimenti, J. C. (2014). Reversal of female infertility by Chk2 ablation reveals the oocyte DNA damage checkpoint pathway. *Science* **343**, 533-536.

Burgoyne, P. S., Mahadevaiah, S. K. and Turner, J. M. A. (2009). The consequences of asynapsis for mammalian meiosis. *Nat. Rev. Genet.* **10**, 207-216.

Canman, C. E., Lim, D. S., Cimprich, K. A., Taya, Y., Tamai, K., Sakaguchi, K., Appella, E., Kastan, M. B. and Siliciano, J. D. (1998). Activation of the ATM kinase by ionizing radiation and phosphorylation of p53. *Science* **281**, 1677-1679.

Celeste, A., Petersen, S., Romanienko, P. J., Fernandez-Capetillo, O., Chen, H. T., Sedelnikova, O. A., Reina-San-Martin, B., Coppola, V., Meffre, E., Difilippantonio, M. J. et al. (2002). Genomic instability in mice lacking histone H2AX. *Science* **296**, 922-927.

Celeste, A., Difilippantonio, S., Difilippantonio, M. J., Fernandez-Capetillo, O., Pilch, D. R., Sedelnikova, O. A., Eckhaus, M., Ried, T., Bonner, W. M. and Nussenzweig, A. (2003). H2AX haploinsufficiency modifies genomic stability and tumor susceptibility. *Cell* **114**, 371-383.

Cloutier, J. M., Mahadevaiah, S. K., Elinati, E., Nussenzweig, A., Tóth, A. and Turner, J. M. A. (2015). Histone H2AFX links meiotic chromosome asynapsis to prophase I oocyte loss in mammals. *PLoS Genet.* **11**, e1005462.

Cole, F., Kauppi, L., Lange, J., Roig, I., Wang, R., Keeney, S. and Jasin, M. (2012). Homeostatic control of recombination is implemented progressively in mouse meiosis. *Nat. Cell Biol.* **14**, 424-430.

Coster, G. and Goldberg, M. (2010). The cellular response to DNA damage: a focus on MDC1 and its interacting proteins. *Nucleus* **1**, 166-178.

Crichton, J. H., Read, D. R., and Adams, I. R. (2017). Defects in Meiotic Recombination Delay Progression Through Pachytene in mouse Spermatocytes. *bioRxiv* doi: https://doi.org/10.1101/102251.

Edelmann, W., Cohen, P. E., Kneitz, B., Winand, N., Lia, M., Heyer, J., Kolodner, R., Pollard, J. W. and Kucherlapati, R. (1999). Mammalian MutS homologue 5 is required for chromosome pairing in meiosis. *Nat. Genet.* **21**, 123-127.

Faieta, M., di Cecca, S., de Rooij, D. G., Luchetti, A., Murdocca, M., di Giacomo, M., di Siena, S., Pellegrini, M., Rossi, P. and Barchi, M. (2016). A surge of late-occurring meiotic double-strand breaks rescues synapsis abnormalities in spermatocytes of mice with hypomorphic expression of SPO11. *Chromosoma* **125**, 189-203.

Fernandez-Capetillo, O., Mahadevaiah, S. K., Celeste, A., Romanienko, P. J., Camerini-Otero, R. D., Bonner, W. M., Manova, K., Burgoyne, P. and Nussenzweig, A. (2003). H2AX is required for chromatin remodeling and inactivation of sex chromosomes in male mouse meiosis. *Dev. Cell* **4**, 497-508.

Fukuda, T., Pratto, F., Schimenti, J. C., Turner, J. M. A., Camerini-Otero, R. D. and Höög, C. (2012). Phosphorylation of chromosome core components may serve as axis marks for the status of chromosomal events during mammalian meiosis. *PLoS Genet.* **8**, e1002485.

Ichijima, Y., Ichijima, M., Lou, Z., Nussenzweig, A., Camerini-Otero, R. D., Chen, J., Andreassen, P. R. and Namekawa, S. H. (2011). MDC1 directs chromosome-wide silencing of the sex chromosomes in male germ cells. *Genes Dev.* **25**, 959-971.

Ichijima, Y., Sin, H.-S. and Namekawa, S. H. (2012). Sex chromosome inactivation in germ cells: emerging roles of DNA damage response pathways. *Cell. Mol. Life Sci.* **69**, 2559-2572.

Jungmichel, S., Clapperton, J. A., Lloyd, J., Hari, F. J., Spycher, C., Pavic, L., Li, J., Haire, L. F., Bonalli, M., Larsen, D. H. et al. (2012). The molecular basis of ATM-dependent dimerization of the Mdc1 DNA damage checkpoint mediator. *Nucleic Acids Res.* **40**, 3913-3928.

Kauppi, L., Barchi, M., Baudat, F., Romanienko, P. J., Keeney, S. and Jasin, M. (2011). Distinct properties of the XY pseudoautosomal region crucial for male meiosis. *Science* **331**, 916-920.

Keeney, S. (2008). Spo11 and the formation of DNA double-strand breaks in meiosis. *Genome Dyn. Stab.* **2**, 81-123.

Keeney, S., Baudat, F., Angeles, M., Zhou, Z.-H., Copeland, N. G., Jenkins, N. A., Manova, K. and Jasin, M. (1999). A mouse homolog of the Saccharomyces cerevisiae meiotic recombination DNA transesterase Spo11p. *Genomics* **61**, 170-182.

Khanna, K. K., Keating, K. E., Kozlov, S., Scott, S., Gatei, M., Hobson, K., Taya, Y., Gabrielli, B., Chan, D., Lees-Miller, S. P. et al. (1998). ATM associates with and phosphorylates p53: mapping the region of interaction. *Nat. Genet.* **20**, 398-400.

Kim, S., Peterson, S. E., Jasin, M. and Keeney, S. (2016). Mechanisms of germ line genome instability. *Semin. Cell Dev. Biol.* **54**, 177-187.

Kneitz, B., Cohen, P. E., Avdievich, E., Zhu, L., Kane, M. F., Hou, H., Jr, Kolodner, R. D., Kucherlapati, R., Pollard, J. W. and Edelmann, W. (2000). MutS homolog 4 localization to meiotic chromosomes is required for chromosome pairing during meiosis in male and female mice. *Genes Dev.* **14**, 1085-1097.

Kolas, N. K., Svetlanov, A., Lenzi, M. L., Macaluso, F. P., Lipkin, S. M., Liskay, R. M., Greally, J., Edelmann, W. and Cohen, P. E. (2005). Localization of MMR proteins on meiotic chromosomes in mice indicates distinct functions during prophase I. *J. Cell Biol.* **171**, 447-458.

La Volpe, A. and Barchi, M. (2012). Meiotic double strand breaks repair in sexually reproducing eukaryotes: we are not all equal. *Exp. Cell Res.* **318**, 1333-1339.

Lam, I. and Keeney, S. (2015). Mechanism and regulation of meiotic recombination initiation. *Cold Spring Harb. Perspect. Biol.* **7**, a016634.

Lange, J., Pan, J., Cole, F., Thelen, M. P., Jasin, M. and Keeney, S. (2011). ATM controls meiotic double-strand-break formation. *Nature* **479**, 237-240.

Lavin, M. F. and Kozlov, S. (2007). ATM activation and DNA damage response. *Cell Cycle* **6**, 931-942.

Lee, A. C., Fernandez-Capetillo, O., Pisupati, V., Jackson, S. P. and Nussenzweig, A. (2005). Specific association of mouse MDC1/NFBD1 with NBS1 at sites of DNA-damage. *Cell Cycle* **4**, 177-182.

Lipkin, S. M., Moens, P. B., Wang, V., Lenzi, M., Shanmugarajah, D., Gilgeous, A., Thomas, J., Cheng, J., Touchman, J. W., Green, E. D. et al. (2002). Meiotic arrest and aneuploidy in MLH3-deficient mice. *Nat. Genet.* **31**, 385-390.

Lou, Z., Minter-Dykhouse, K., Franco, S., Gostissa, M., Rivera, M. A., Celeste, A., Manis, J. P., van Deursen, J., Nussenzweig, A., Paull, T. T. et al. (2006). MDC1 maintains genomic stability by participating in the amplification of ATM-dependent DNA damage signals. *Mol. Cell* **21**, 187-200.

Lu, W.-J., Chapo, J., Roig, I. and Abrams, J. M. (2010). Meiotic recombination provokes functional activation of the p53 regulatory network. *Science* **328**, 1278-1281.

Lynn, A., Soucek, R. and Börner, G. V. (2007). ZMM proteins during meiosis: crossover artists at work. *Chromosome Res.* **15**, 591-605.

Mahadevaiah, S. K., Bourc'his, D., de Rooij, D. G., Bestor, T. H., Turner, J. M. A. and Burgoyne, P. S. (2008). Extensive meiotic asynapsis in mice antagonises meiotic silencing of unsynapsed chromatin and consequently disrupts meiotic sex chromosome inactivation. *J. Cell Biol.* **182**, 263-276.

Marcet-Ortega, M., Pacheco, S., Martínez-Marchal, A., Castillo, H., Flores, E., Jasin, M., Keeney, S. and Roig, I. (2017). p53 and TAp63 participate in the recombination-dependent pachytene arrest in mouse spermatocytes. *PLoS Genet.* **13**, e1006845.

Matsuoka, S., Ballif, B. A., Smogorzewska, A., Mcdonald, E. R., Ill, Hurov, K. E., Luo, J., Bakalarski, C. E., Zhao, Z., Solimini, N., Lerenthal, Y. et al. (2007). ATM and ATR substrate analysis reveals extensive protein networks responsive to DNA damage. *Science* **316**, 1160-1166.

Moens, P. B., Kolas, N. K., Tarsounas, M., Marcon, E., Cohen, P. E. and Spyropoulos, B. (2002). The time course and chromosomal localization of recombination-related proteins at meiosis in the mouse are compatible with models that can resolve the early DNA-DNA interactions without reciprocal recombination. *J. Cell Sci.* **115**, 1611-1622.

Moens, P. B., Marcon, E., Shore, J. S., Kochakpour, N. and Spyropoulos, B. (2007). Initiation and resolution of interhomolog connections: crossover and non-crossover sites along mouse synaptonemal complexes. *J. Cell Sci.* **120**, 1017-1027.

Muciaccia, B., Boitani, C., Berloco, B. P., Nudo, F., Spadetta, G., Stefanini, M., de Rooij, D. G. and Vicini, E. (2013). Novel stage classification of human spermatogenesis based on acrosome development. *Biol. Reprod.* **89**, 60.

Neale, M. J., Pan, J. and Keeney, S. (2005). Endonucleolytic processing of covalent protein-linked DNA double-strand breaks. *Nature* **436**, 1053-1057.

Pacheco, S., Marcet-Ortega, M., Lange, J., Jasin, M., Keeney, S. and Roig, I. (2015). The ATM signaling cascade promotes recombination-dependent pachytene arrest in mouse spermatocytes. *PLoS Genet.* **11**, e1005017.

Pan, J., Sasaki, M., Kniewel, R., Murakami, H., Blitzblau, H. G., Tischfield, S. E., Zhu, X., Neale, M. J., Jasin, M., Socci, N. D. et al. (2011). A hierarchical combination of factors shapes the genome-wide topography of yeast meiotic recombination initiation. *Cell* **144**, 719-731.

Perry, J., Palmer, S., Gabriel, A. and Ashworth, A. (2001). A short pseudoautosomal region in laboratory mice. *Genome Res.* **11**, 1826-1832.

Pittman, D. L., Cobb, J., Schimenti, K. J., Wilson, L. A., Cooper, D. M., Brignull, E., Handel, M. A. and Schimenti, J. C. (1998). Meiotic prophase arrest with failure of chromosome synapsis in mice deficient for Dmc1, a germline-specific RecA homolog. *Mol. Cell* **1**, 697-705.

Rass, E., Chandramouly, G., Zha, S., Alt, F. W. and Xie, A. (2013). Ataxia telangiectasia mutated (ATM) is dispensable for endonuclease I-SceI-induced homologous recombination in mouse embryonic stem cells. *J. Biol. Chem.* **288**, 7086-7095.

Reynolds, A., Qiao, H., Yang, Y., Chen, J. K., Jackson, N., Biswas, K., Holloway, J. K., Baudat, F., de Massy, B., Wang, J. et al. (2013). RNF212 is a dosage-sensitive regulator of crossing-over during mammalian meiosis. *Nat. Genet.* **45**, 269-278.

Rogakou, E. P., Pilch, D. R., Orr, A. H., Ivanova, V. S. and Bonner, W. M. (1998). DNA double-stranded breaks induce histone H2AX phosphorylation on serine 139. *J. Biol. Chem.* **273**, 5858-5868.

Rogakou, E. P., Boon, C., Redon, C. and Bonner, W. M. (1999). Megabase chromatin domains involved in DNA double-strand breaks in vivo. *J. Cell Biol.* **146**, 905-916.

Royo, H., Polikiewicz, G., Mahadevaiah, S. K., Prosser, H., Mitchell, M., Bradley, A., de Rooij, D. G., Burgoyne, P. S. and Turner, J. M. A. (2010). Evidence that meiotic sex chromosome inactivation is essential for male fertility. *Curr. Biol.* **20**, 2117-2123.

Royo, H., Prosser, H., Ruzankina, Y., Mahadevaiah, S. K., Cloutier, J. M., Baumann, M., Fukuda, T., Hoog, C., Toth, A., de Rooij, D. G. et al. (2013). ATR acts stage specifically to regulate multiple aspects of mammalian meiotic silencing. *Genes Dev.* **27**, 1484-1494.

Russell, L. D., Ettlin, R. A., Hikim, A. P. S. and Clegg, E. D. (1990). *Histological and Histopatological Evaluation of the Testis*. Clerwater, FL: Cache River Press.

Santucci-Darmanin, S., Walpita, D., Lespinasse, F., Desnuelle, C., Ashley, T. and Paquis-Flucklinger, V. (2000). MSH4 acts in conjunction with MLH1 during mammalian meiosis. *FASEB J.* **14**, 1539-1547.

Silva, N., Adamo, A., Santonicola, P., Martinez-Perez, E. and La Volpe, A. (2013). Pro-crossover factors regulate damage-dependent apoptosis in the Caenorhabditis elegans germ line. *Cell Death Differ.* **20**, 1209-1218.

Snowden, T., Acharya, S., Butz, C., Berardini, M. and Fishel, R. (2004). hMSH4-hMSH5 recognizes Holliday Junctions and forms a meiosis-specific sliding clamp that embraces homologous chromosomes. *Mol. Cell* **15**, 437-451.

Sonoda, E., Zhao, G. Y., Kohzaki, M., Dhar, P. K., Kikuchi, K., Redon, C., Pilch, D. R., Bonner, W. M., Nakano, A., Watanabe, M. et al. (2007). Collaborative roles of gammaH2AX and the Rad51 paralog Xrcc3 in homologous recombinational repair. *DNA Repair* **6**, 280-292.

Stewart, G. S., Wang, B., Bignell, C. R., Taylor, A. M. R. and Elledge, S. J. (2003). MDC1 is a mediator of the mammalian DNA damage checkpoint. *Nature* **421**, 961-966.

Storlazzi, A., Gargano, S., Ruprich-Robert, G., Falque, M., David, M., Kleckner, N. and Zickler, D. (2010). Recombination proteins mediate meiotic spatial chromosome organization and pairing. *Cell* **141**, 94-106.

Svetlanov, A., Baudat, F., Cohen, P. E. and de Massy, B. (2008). Distinct functions of MLH3 at recombination hot spots in the mouse. *Genetics* **178**, 1937-1945.

Ünal, E., Arbel-Eden, A., Sattler, U., Shroff, R., Lichten, M., Haber, J. E. and Koshland, D. (2004). DNA damage response pathway uses histone modification to assemble a double-strand break-specific cohesin domain. *Mol. Cell* **16**, 991-1002.

Xie, A., Puget, N., Shim, I., Odate, S., Jarzyna, I., Bassing, C. H., Alt, F. W. and Scully, R. (2004). Control of sister chromatid recombination by histone H2AX. *Mol. Cell* **16**, 1017-1025.

Xie, A., Hartlerode, A., Stucki, M., Odate, S., Puget, N., Kwok, A., Nagaraju, G., Yan, C., Alt, F. W., Chen, J. et al. (2007). Distinct roles of chromatin-associated proteins MDC1 and 53BP1 in mammalian double-strand break repair. *Mol. Cell* **28**, 1045-1057.

Xie, A., Odate, S., Chandramouly, G. and Scully, R. A. (2010). H2AX post-translational modifications in the ionizing radiation response and homologous recombination. *Cell Cycle* **9**, 3602-3610.

Yoshida, K., Kondoh, G., Matsuda, Y., Habu, T., Nishimune, Y. and Morita, T. (1998). The mouse RecA-like gene Dmc1 is required for homologous chromosome synapsis during meiosis. *Mol. Cell* **1**, 707-718.

Yuan, J., Adamski, R. and Chen, J. (2010). Focus on histone variant H2AX: to be or not to be. *FEBS Lett.* **584**, 3717-3724.

Zhang, J., Ma, Z., Treszezamsky, A. and Powell, S. N. (2005). MDC1 interacts with Rad51 and facilitates homologous recombination. *Nat. Struct. Mol. Biol.* **12**, 902-909.